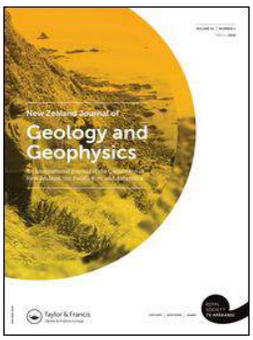

New Zealand Journal of Geology and Geophysics

ISSN: (Print) (Online) Journal homepage: https://www.tandfonline.com/loi/tnzg20

Lateral, longitudinal, and temporal variation in trench-slope basin fill: examples from the Neogene Akitio sub-basin, Hikurangi Margin, New Zealand

Adam D. McArthur, Julien Bailleul, Frank Chanier, Alan Clare & William D. McCaffrey

To cite this article: Adam D. McArthur, Julien Bailleul, Frank Chanier, Alan Clare & William D. McCaffrey (2021): Lateral, longitudinal, and temporal variation in trench-slope basin fill: examples from the Neogene Akitio sub-basin, Hikurangi Margin, New Zealand, New Zealand Journal of Geology and Geophysics, DOI: 10.1080/00288306.2021.1977343

To link to this article: https://doi.org/10.1080/00288306.2021.1977343

Published online: 06 Oct 2021.

NEW ZEALAND JOURNAL OF GEOLOGY AND GEOPHYSICS
https://doi.org/10.1080/00288306.2021.1977343

Taylor & Francis
Taylor & Francis Group

RESEARCH ARTICLE

OPEN ACCESS Check for updates

Lateral, longitudinal, and temporal variation in trench-slope basin fill: examples from the Neogene Akitio sub-basin, Hikurangi Margin, New Zealand

Adam D. McArthur[a], Julien Bailleul[b], Frank Chanier[c], Alan Clare[d] and William D. McCaffrey[a]

[a]School of Earth and Environment, University of Leeds, Leeds, UK; [b]Geosciences Department, U2R 7511, Basins-Reservoirs-Resources (B2R), UniLaSalle, Beauvais, France; [c]Laboratory of Oceanology and Geosciences (LOG), University of Lille, CNRS, ULCO, UMR 8187, Lille, France; [d]OMV New Zealand Ltd Wellington, New Zealand

ABSTRACT

The fill of trench-slope basins is complex, varying temporally, laterally, and longitudinally. New data from the Neogene stratigraphy of the Akitio Sub-basin, Wairarapa, are presented to investigate such fill variation. The preserved basin fill spans an area 70 km long by 10 km wide, representing deposits from a trench-slope basin. Integration of sedimentological, micropalaeoentological, and geological mapping data charts basin fill evolution. Over 15 km of strata were logged, defining 17 lithofacies associations, which were mapped across the basin; these are interpreted to represent both shallow and deep-water environments. The deep-water strata show a temporal evolution from ponded turbidite deposition, to a period of basin spill via conduits connecting to downstream basins, development of aggradational channel-levees, and finally unconfined submarine fan deposition. Shallow marine deposits mostly developed on the up-dip basin margin occur contemporaneously with basinal mass-transport deposits, and in association with the growth of basin bounding structural ridges. Comparison with the evolution of the offshore, actively filling Akitio Trough highlights controls on trench-slope basin fill: a first-order influence of external controls, e.g. tectonism to create the basin; a second-order progression from under- to overfilled; and third-order lateral variation reflecting autogenic process and the effects of local structures on seafloor gradients. These factors combine to vary sedimentation in trench-slope-basins spatially and temporally.

ARTICLE HISTORY
Received 15 June 2021
Accepted 2 September 2021

HANDLING EDITOR
Kyle Bland

KEYWORDS
Miocene; turbidites; ponded; lobes; channels; bypass; confined; unconfined

Introduction

Understanding the fill of trench-slope basins is not straightforward, given the complex structural setting, the fact that not many are exhumed at outcrop, and that strata vary laterally and longitudinally depending on a multitude of influences (Underwood and Moore 1995; Morley et al. 2011). However, deep-water fold and thrust belts often comprise major, self-contained petroleum systems, e.g. the Sinú, offshore Colombia (Vinnels et al. 2010); act as sinks of sediment including organic carbon, e.g. in the Japan Trench system (von Huene et al. 1982); the type of sediment is fundamental in controlling the nature of the deformation (Butler 2019); and, in turn, the sedimentation records the tectonic history and its study may help to reconstruct the margin evolution.

Building stratigraphic models to help predict lithofacies distribution in the subsurface is crucial, particularly in trench-slope systems, where events in up-dip basins may be reflected in downstream portions of the margin (Morley et al. 2011). Seismic scale studies can indicate the overall architecture but provide little direct constraint on the lithology, lithofacies distribution, and reservoir quality occurring in the seismically imaged systems. The nature of these structurally evolving basins may lead to a variety of depositional systems and recognition of architectural elements, lithofacies distribution, and indicators of bypass are essential to constrain construction of the margin (Stevenson et al. 2015; Sylvester et al. 2015; Crisóstomo-Figueroa et al. 2020).

The offshore trench-slope basins of the Hikurangi Margin present an excellent opportunity to study actively filling trench-slope basins. However, lacking sufficient well control (Figure 1), little can be said regarding the style of sedimentary rocks in the offshore basins. Hence the need for this study to define the lithofacies present in the interior, outcropping basins and to build architectural models for the stratigraphic evolution of trench-slope basins. Furthermore, the onshore basins may have lain on the same sediment pathway as offshore basins, and so give indications of timing of downstream sediment bypass. Here we examine Neogene outcrops of the Akitio Sub-basin from the exhumed portion of Hikurangi Margin on the North Island, New Zealand (Figure 1).

Although previous studies have documented the broad stratigraphy of the onshore basins (Ongley

CONTACT Adam D. McArthur A.McArthur@leeds.ac.uk

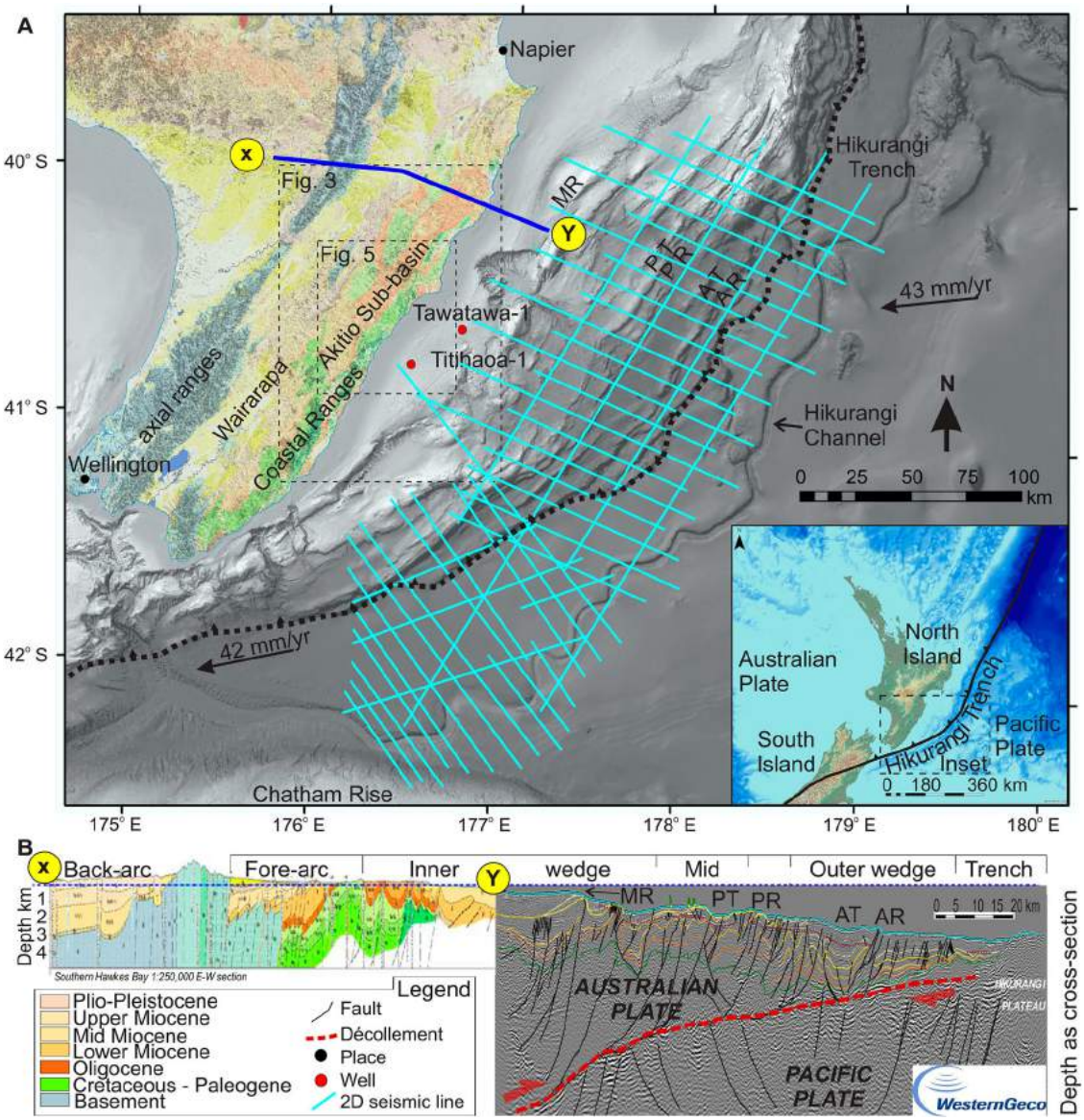

Figure 1. A, Hikurangi Margin onshore geological map (Heron 2014) and offshore bathymetry (courtesy of NIWA). **B,** Integration of geological cross section (modified from Lee and Begg 2002) and interpreted, depth migrated seismic line courtesy of WesternGeco, both at same vertical and horizontal scale, with ×4 vertical exaggeration. AT = Akitio Trough; AR = Akitio Ridge; MR = Motuokura Ridge; PT = Porangahau Trough; PR = Porangahau Ridge.

1935; Kingma 1958; Neef 1967; Johnston 1980; Van Der Lingen and Pettinga 1980; Neef 1981, 1991; Neef and Bottrill 1992; Neef 1992a; 1992b; 1995; 1997; 1999a; 1999b; Reid 1998), much of this work focused on identifying broad stratigraphic elements, whilst recent studies have concentrated on a trench-perpendicular transect of the Akitio Sub-basin (Bailleul et al. 2007, 2013). In order to fully understand the fill of a trench-slope basin and implications for downstream basins, it is essential to understand the full distribution of lithofacies and architectural elements, both temporally and spatially across a basin. This study aims to provide a lithostratigraphic framework for the Akitio Sub-basin. Specific objectives are to: (1) Log, define, and map the Neogene sedimentary rocks in the exhumed Akitio Sub-basin. (2) Use the field data and information from previous studies to (a) Build an integrated model of basin fill development and evolution, including (i) Characterise spatial variations in lithofacies and architecture distribution. (ii) Identify key unconformities and bypass surfaces. (iii) Incorporate insights from the regional geological setting and from the offshore actively developing basins, (b) Assess the implications for linked, downstream basin development. (3) Develop predictive models for the stratigraphic evolution of trench-slope basins.

Geological setting

This study concerns the Neogene sequence of the Hikurangi subduction margin (Figure 1). Before the onset of Cenozoic subduction, most of Zealandia (i.e. the New Zealand microcontinent) was submerged (Reyners 2013; Strogen et al. 2014). The region that would become the Hikurangi Margin was

then a dormant margin, with deposition of Paleogene deep-marine carbonates and marls (Figure 2; Lillie 1953; Chanier and Ferriere 1991). Hikurangi subduction initiated ca. 25 Ma, by convergence of the Australian and Pacific plates (Figure 1; Rait et al. 1991; Nicol et al. 2007; Jiao et al. 2014). Subduction formed the Hikurangi Trench, which defines the eastern limit of the margin and the axial ranges of the North Island that defines the western limit (Figure 1; Brodie and Hatherton 1958; Ballance 1976; McArthur and Tek 2021). Extensive deformation of the overriding Australian Plate during the Neogene entailed major, often out-of-sequence, ENE-WSW striking thrust faulting, with subordinate normal and dextral faulting (Figure 1; Chanier and Ferriere 1991; Beanland et al. 1998; Nicol et al. 2007; Barnes et al. 2010). NE-SW elongated trench-slope basins have formed between major thrust cored structures atop the subduction wedge (Lewis and Pettinga 1993; Bailleul et al. 2013; McArthur et al. 2020).

Neogene deformation can be separated into three phases (Figure 2; Wells 1989; Chanier and Ferriere 1991; Rait et al. 1991; Chanier et al. 1999), comprising: (P1) Early Miocene compression, uplift and emplacement of thrust nappes (Chanier and Ferriere 1991). (P2) A Middle to Late Miocene phase of extension and compression, with subsidence and normal faulting in the interior resulting from tectonic collapse-related extension (Chanier et al. 1999; Barnes et al. 2002; Bailleul et al. 2013). (P3) Latest Miocene to present-day resumption of margin-wide compression, with further thrusting and uplift, resulting in the present-day fold and thrust belt and frontal accretion (Nicol and Beavan 2003; Litchfield et al. 2007; Nicol et al. 2007; Bailleul et al. 2013; McArthur et al. 2020). A series of active strike-slip faults transect the upper plate (Figure 3); however, these are inferred to be relatively recent, with reverse and normal faults being largely responsible for syn-sedimentary activity in the basin (Beanland et al. 1998; Lee and Begg 2002; Nicol et al. 2007). Major basin bounding structures, such as the Adams-Tinui Fault Zone and the Whakataki Fault were periodically active from the onset of Neogene deformation (Chanier and Ferriere 1991; Rait et al. 1991; Neef 1992a; Bailleul et al. 2007). Indeed they likley exploited older structures (Pettinga 1982; McArthur et al. 2020) and have shown variable styles of deformation, i.e. thrusting, normal and strike-slip through their history (Chanier et al. 1999; Malié et al. 2017).

The tectonostratigraphic evolution of the subduction wedge is recorded in the filling of the trench-slope basins, which was diachronous; the innermost have a Miocene aged fill, with generally younger deposits towards the trench (Figure 2; Lewis and Pettinga 1993). Marine sedimentation predominates in the trench-slope basins (Van Der Lingen and Pettinga 1980; Neef 1992a; Field et al. 1997; Bailleul et al. 2007), the record of which exhibits a marked tectonic control, with sedimentations disrupted by a series of dis- and unconformities (Neef 1992a; Bailleul et al. 2007, 2013; Burgreen and Graham 2014; Burgreen-Chan et al. 2016; McArthur and McCaffrey 2019; McArthur et al. 2021). The fill of the basins includes widespread deep-marine marls, mudstones, turbidites, contourites, mass-transport deposits, and shallow marine siliciclastics and carbonates (Figure 2; Lee and Begg 2002; McArthur et al. 2020; Clausmann et al. 2021).

The studied strata crop out within the ~70 km long by 10 km wide Akitio Synclinorium, the Tawhero and Waihoki synclines, and the Puketoi Monocline (Figure 3; Neef 1992b), which corresponds to the preserved remnants of the Akitio Sub-basin fill (Bailleul et al. 2007). The basin is constrained by structural 'blocks'; to the northwest by the Pongaroa Block and to the southeast by the Coastal Block (Figure 3), both exposing pre-subduction 'basement'. The limits of the blocks are defined by the Pongaroa Fault to the NW and by the Adams-Tinui Fault Zone to the SE (Figure 3; Neef 1997, 1999a; Bailleul et al. 2007). Although unlikely to have been continually active over the past ~25 Ma, these faults demonstrate activity from the earliest Miocene into the Pleistocene (Bailleul et al. 2013; Malié et al. 2017). These blocks were drowned during Late Miocene expansion of the depocentre (Bailleul et al. 2013). The resulting enlarged depocentre has been referred to as the Tawhero Basin (Neef 1997), essentially marking a change in structural style, subsidence rates, and stratigraphy of the basin during the Late Miocene (Bailleul et al. 2013). Here we simply refer to the Miocene basin as the Akitio Sub-basin.

Although relatively undeformed, the basin is cut by the N-S trending Breakdown Fault Zone (Figure 3; Neef 1992b; Malié et al. 2017), whilst the Auster and Paripapa synclines, and the Kawakawa Anticline represent subordinate folding (Figure 3; Ongley 1935). The three phases of deformation defined above are recorded in the sediment style and distribution in the basin, deformation and migration of the basin edges, and unconformities (Bailleul et al. 2013). A very complex local stratigraphic nomenclature has been somewhat simplified by Lee and Begg (2002); this study focuses on the lithofacies.

Methodology

High resolution, bed-for-bed scale (1:50) logging was conducted at a number of key locations through the basin, totalling ~15 km of measured sections (Figure 4). Numerous (>1150) palaeocurrent directions were collected from 3D surfaces in all measured sections. Photomosaics of key outcrops were taken to document the stratigraphic architecture. This allowed a rigorous lithofacies scheme to be developed (Table 1)

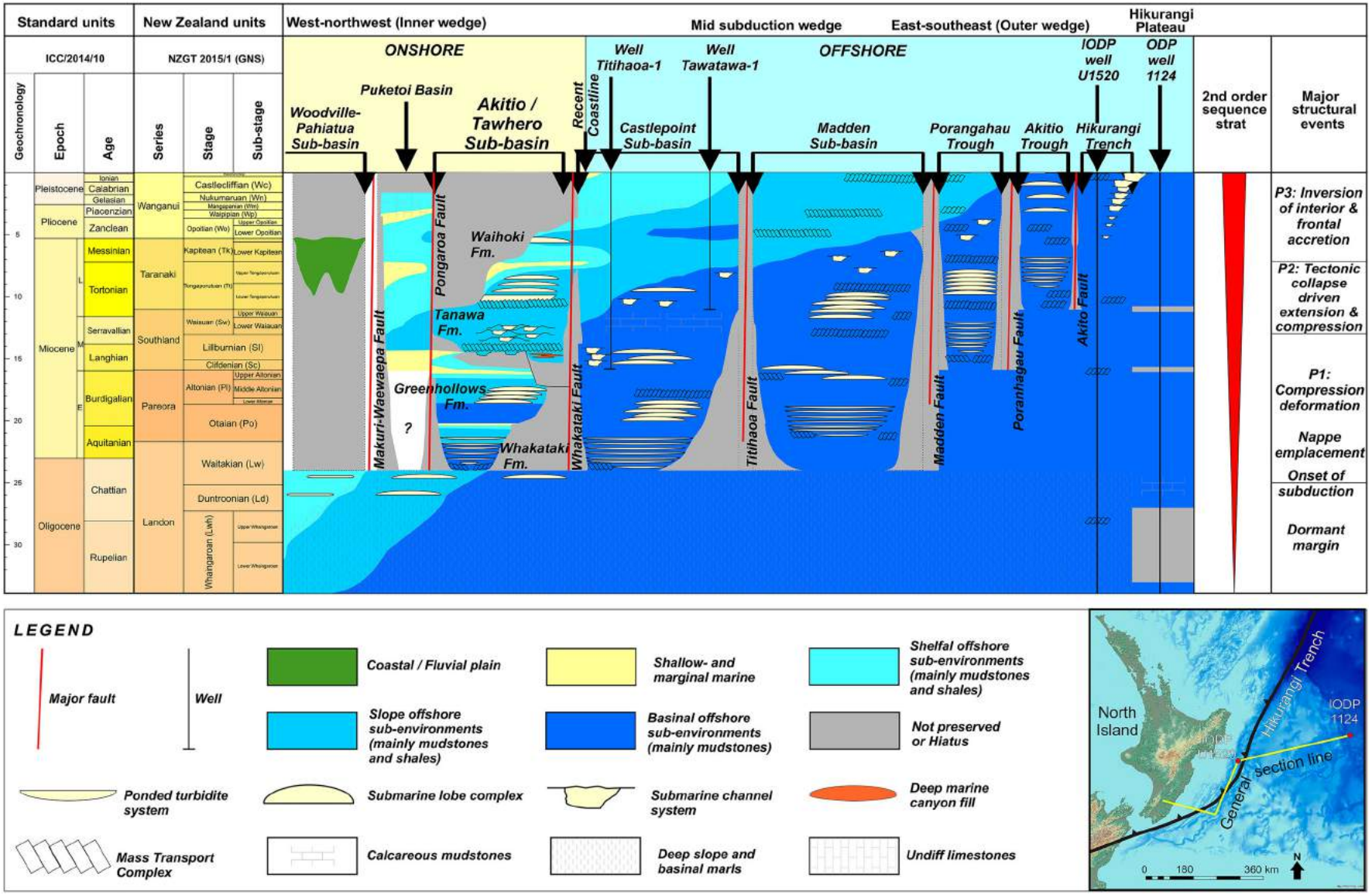

Figure 2. Tectono-stratigraphy of the Hikurangi Margin (modified from Uruski 1997; Tap Oil Limited 2004; Bailleul et al. 2013; Bland et al. 2015; Burgreen-Chan et al. 2016; Barnes et al. 2020 and McArthur et al. 2021). Regional tectonism adapted from Rait et al. (1991), Lewis and Pettinga (1993), Chanier et al. (1999), Lee and Begg (2002), Nicol et al. (2007) and Reyners (2013). International time scale after Cohen et al. (2013), New Zealand stages after Raine et al. (2015).

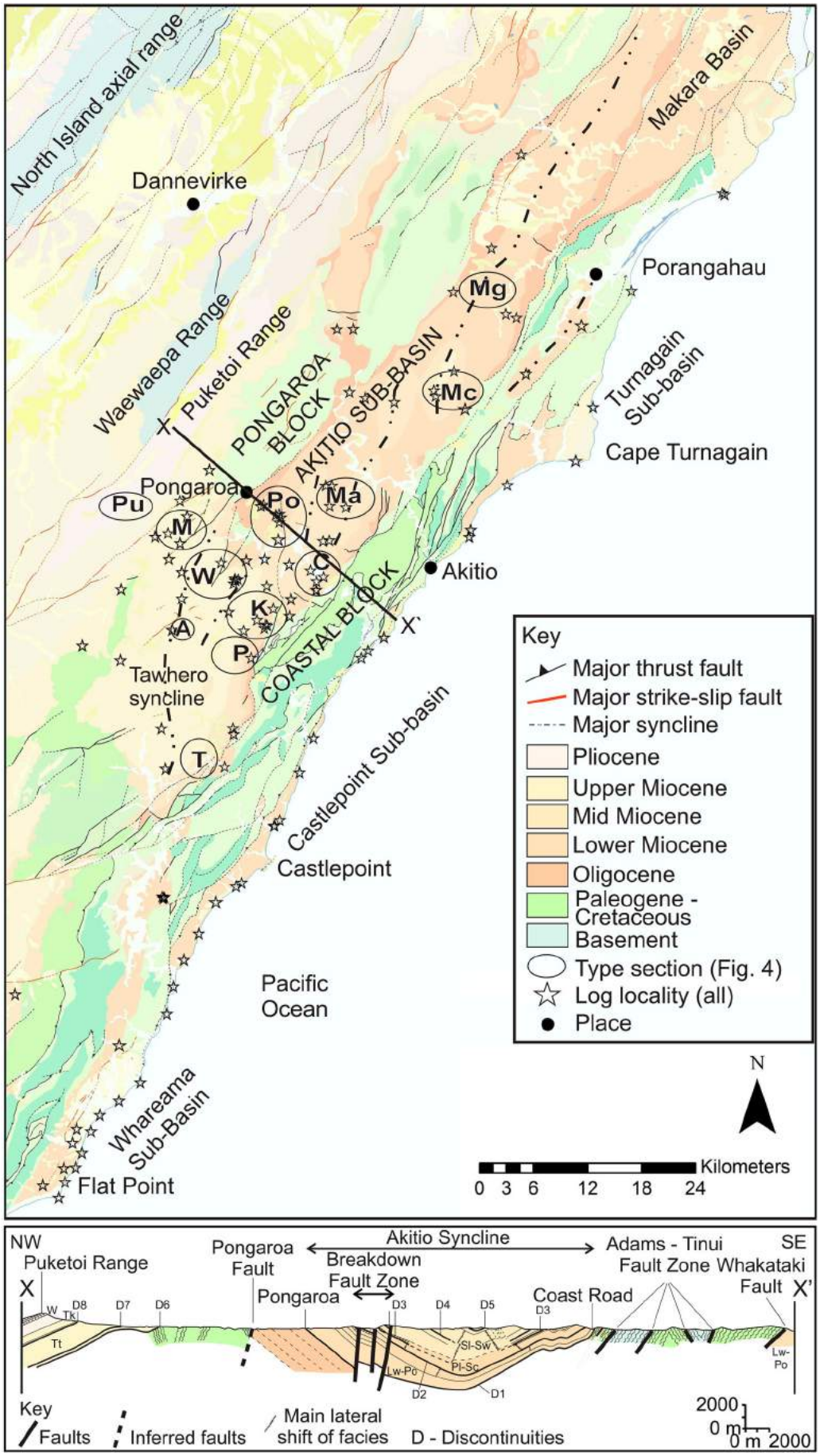

Figure 3. Geological map of the Akitio Sub-basin with full range of log locations from this research and schematic cross section X-X`. Names of type sections as Figure 4. Modified from Lee and Begg (2002) and Bailleul et al. (2013).

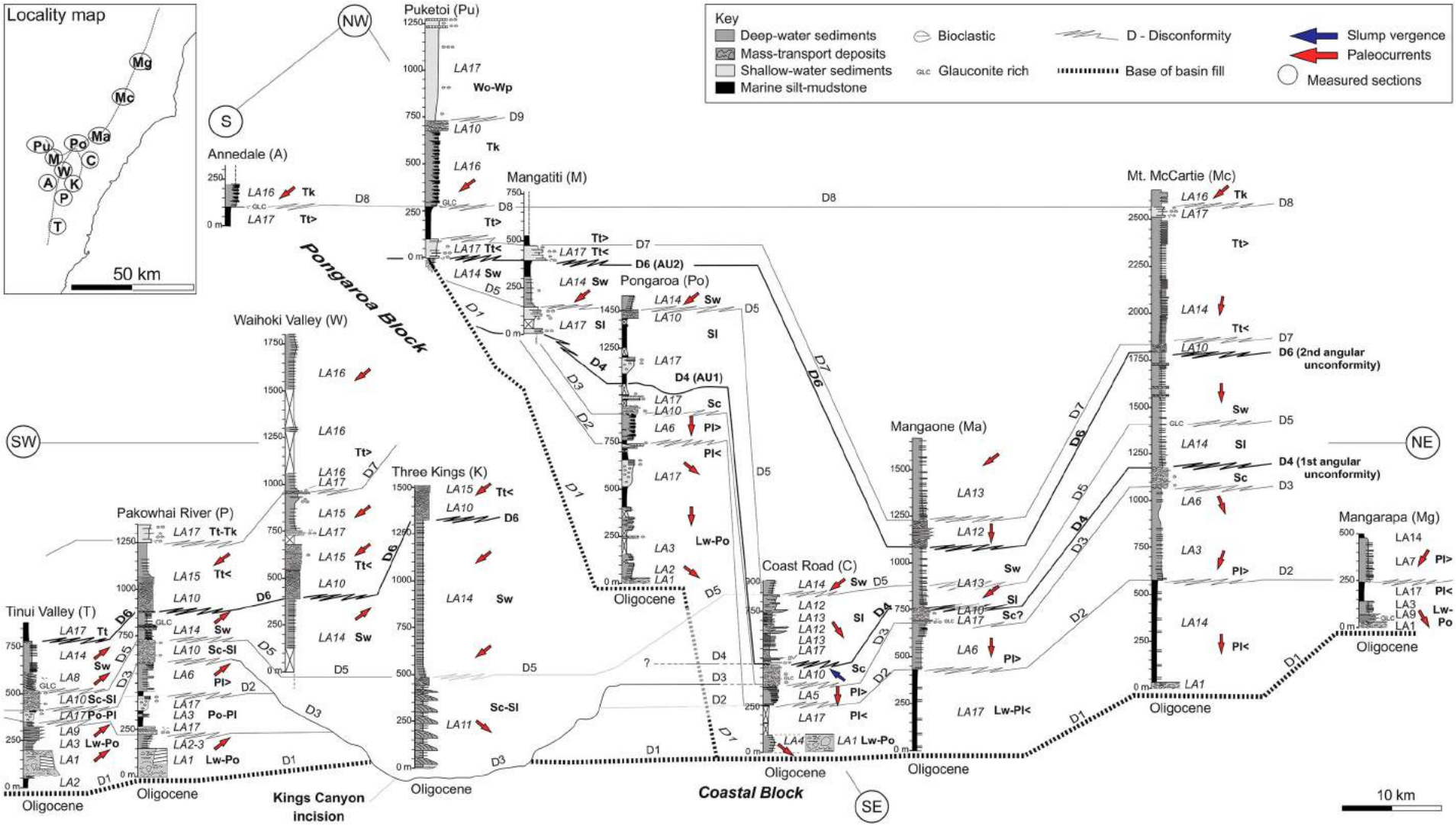

Figure 4. Fence correlation diagram from W-E and S-N through the Akitio Sub-basin. LA = Lithofacies association. For age codes refer to Figure 2. Disconformities (D) after Bailleul et al. (2013).

Table 1. Lithofacies of the Akitio Sub-basin.

Lithofacies type	Grain size & bed thickness	Observations	Interpretation
LF1 – Muddy debrite (Figure 7C)	Silty mudstone matrix with floating pebbles to cobbles; beds less than 50 cm thick	Medium grey, chaotic, structure- less mudstone with concentrations of silt- to sand grade material, very fragmented bioclastic material (often at the base) and rare exotic and mud-clasts. Beds often seen to infill significant scours (decimetre) into underlying strata. No bioturbation observed. Typically occurs with irregular thin-beds (LF9).	Interpreted as mud-rich debrites (*sensu* Crowell 1957), depositing material remobilised from up-dip. This can be locally derived, e.g., channel margins or relatively long distance, e.g., from shelfal areas.
LF2 – Matrix supported polymict conglomerate (Figure 7D)	Pebble to boulder sized clasts set within granular to fine grained matrix; beds are typically up to 150 cm thick, but in rare cases may be tens of m thick	Typically chaotic, very poorly-sorted and organised, massive conglomerates. Bed bases are typically sharp and erosive, often scouring tens of centimetres. Subtle cross-stratification rarely observed. Beds typically laterally very variable in thickness, discontinuous and may laterally grade into thin sandstones (Lee and Begg 2002). May show normal, inverse or no grading from pebbles to boulders, which range from spherical to angular and spheroidal to elongate. Rarely includes outsized rafts of material up to 20 m long. Clasts represent a wide range of lithologies, including older formations, such as Whangai, Wanstead and Weber formations or rarely Torlesse greywacke and may show a subordinate proportion of "intraformational" sandstone, carbonate or mudstone clasts. Clasts typically represent <50% of beds, being matrix supported, hence imbrications are rare. Matrix typically consists of a poorly sorted granular to very fine-grained sandstone, often with a bioclastic component. Wood debris was rarely found.	Interpreted to represent the products of submarine debris flows. Different beds may show different concentrations of clast types, indicating variable sources and potential mixing of lithologies during transport. Delteil et al. (2006) considered these to represent mass-failures of fault scarps at the basin margin. Claussmann et al. (2021) provide a thorough description of this facies.
LF3 – Clast supported polymict conglomerate (Figure 7B)	Pebble to boulder sized clasts set within granular to fine grained matrix; beds are up to 240 cm thick	Typically chaotic, very poorly sorted, massive conglomerates. Bed bases typically sharp and erosive, often scouring tens of centimetres. Subtle cross-stratification rarely observed in a minority of beds, which are normally laterally restricted to a few tens of m. May show normal, inverse or no grading from pebbles to boulders, which range from spherical to angular and spheroidal to elongate. Clasts may show imbrications. Clasts represent a wide range of lithologies, including older lithologies, such as Whangai, Wanstead and Weber formations or Torlesse greywacke. Clasts typically represent less than 70% of the bed, but show clast contacts and are considered clast supported. Matrix typically consists of poorly sorted granular to very fine-grained sandstone, often with a bioclastic component and rare wood debris.	Interpreted to represent the products of submarine debris flows. When associated with turbidites, these may also be interpreted to represent the traction carpet of high-density turbidity currents (R2-3 of Lowe 1982) and include the Packspur Conglomerate, which Neef (1992a) interpreted to have filled a submarine channel. Claussmann et al. (2021) provide a detailed description of this facies.
LF4 – Monomict conglomerate (Figure 7A)	Pebble to boulder sized clasts set within granular to fine grained matrix; beds are typically up to 100 cm thick	Typically chaotic, poorly-sorted, massive conglomerates. Bed bases are sharp, erosive and may show subtle erosion. Beds usually tabular and more laterally extensive than LF2-3. May show normal, inverse or no grading from pebbles to boulders, which are normally angular and more elongate than LF2-3. Clasts rarely show imbrication. Clasts represent a range of lithologies, including older lithologies, such as Whangai or Weber formations. Clasts represent upwards of 70% of the bed, when showing clast contacts are considered clast supported, but can be matrix supported. Matrix usually consists of a poorly sorted granular to very fine-grained sandstone, occasionally with a bioclastic component.	Although similar to the above lithofacies, clasts here are composed of only one lithology, implying derivation from a local source, e.g. uplifted bedrock. They are also interpreted as the products of debris flows (sensu Crowell 1957).
LF5 – Marl (Figure 7A)	Mud; thin (1 cm) to very thick (<200 cm)	Pale blue-grey, calcareous claystone in beds up to 2 m thick, which amalgamate into packages tens to hundreds of m thick. Bioturbation typically moderate to intense, often resulting in a mottled appearance. Organic matter or shells may be found, but body fossils are very rare.	This calcareous claystone is interpreted to represent background sedimentation in an open marine environment. Given the bioturbation this likely occurred in a shelf to slope setting. Deformation represents remobilisation or tectonic damage.

(*Continued*)

Table 1. Continued.

Lithofacies type	Grain size & bed thickness	Observations	Interpretation
		Often exhibits deformation, including extensive fracture patterns and slide scars.	
LF6 – Hemipelagic mudstone (Figures 8–9)	Mud; thin (1 cm) to very thick (<75 cm)	Light to dark grey mudstone in beds up to 75 cm thick, which often amalgamate into packages m to tens of m thick. Beds are typically laterally continuous at outcrop scale. Bedding is recognised by broad colour changes and/or concreated horizons. Typically exhibits a blocky texture, with a conchoidal fracture. Rarely shows small macrofossils, such as *Inerocamerus* sp. molluscs or macro foraminifera (e.g. *Bathysiphon* sp.). Fragments of organic matter often disseminated and beds may show bioturbation, with horizontal burrows such as *Nerities* sp. and *Phycosiphon* sp. Large and small scale deformation is often evident.	This massive, blocky, mudstone is interpreted to represent background hemipelagic sedimentation in deep-water. Deformation, interpreted as slumps and slide scars, implies deposition on an unstable slope, with remobilisation of gravitationally unstable sediment.
LF7 – Turbidite mudstone (Figures 8–10)	Silty mud; thin (1 cm) to thick (<50 cm)	Dark grey, silty mudstones, occasionally laminated, rich in organic matter, often with visible plant fragments, may show bioturbation, with horizontal burrows (e.g. *Nerities* sp.) and or sub-vertical burrows (e.g. *Ophiomorpha* sp.or *Thalassinoides* sp.). Beds are typically laterally continuous over outcrop scale, but may show significant lateral thickness variations. Typically occurs above LF8 and below LF6.	This organic rich, silty, often laminated mudstone is interpreted as the fallout from suspension clouds of turbidity currents (Bouma Te).
LF8 – Turbidite siltstone (Figures 8–9)	Silt; thin (1 cm) to medium (<20 cm)	Pale grey siltstone. Typically organic rich, may be massive or with planar and ripple cross lamination. Beds may show good lateral continuity. Bed bases typically gradational from underlying sandstones or sharp over LF6 mudstone and grade into LF7.	These siltstones represent current reworking of suspension cloud fallout from weak low-density turbidity currents (Bouma Td). Massive intervals are likely extensively bioturbated.
LF9 – Laterally variable thin- to medium-bedded sandstone (Figure 8E)	Fine to very fine (very rarely medium) grained; thin to medium-bedded (<20 cm)	Pale grey to beige, well-sorted sandstone. Typically shows a sharp, irregular base, occasionally lower portion of beds show planar laminations and upper portions may show ripples and cross-lamination. Beds not always normally graded and may show variation in order of structures. Beds may show significant lateral variation in thickness or occur as lenses. May be rich in carbonaceous material, often highlighting planar and ripple lamination. Sandstones are typically texturally immature, displaying a variety of lithic fragments and glauconite. Bioturbation is variable and macrofossils not observed. Typically proceeded by LF6 or LF7.	Deposition from dilute, low-density turbidity currents (Bouma Tc-d). Traction structures imply deposition from waning flows. Lateral variation may be a result of thinning and pinch out against a confining surface when apparent or when lens shaped, to have infilled a scour surface. When filling scours and directly overlain by hemipelagic (LF6) mudstone inferred to have a bypass component (*sensu* Stevenson et al. 2015).
LF10 – Laterally persistent thin- to medium-bedded sandstone (Figure 8)	Fine to very fine (very rarely medium) grained; thin to medium-bedded (<20 cm)	Pale grey to beige, normally graded, typically well-sorted sandstone. Bed bases may be sharp or slightly irregular with sole marks including tool marks and flutes. Beds are tabular and traceable over hundreds of m. Lower portion of beds may show planar lamination, often highlighted by organic rich bands; beds typically subtly grade up and often show a dewatered and/or massive middle interval; bed tops typically current rippled and grade to siltstone (LF8); this is an idealised succession and beds may show a different order or not all intervals. Ripples may show a subtly different orientation to sole structures and infrequently show variations between rippled horizons in the same bed. Very rarely, climbing ripples occur. Bioturbation is variably absent to intense, particularly in bed tops which may show a mottled texture.	These sandstones, with a variety of traction structures are interpreted as the deposition from low-density turbidity currents (Bouma Tb-c). The normal succession of structures and continuity of beds implies deposition from waning flows. Variations in order of sedimentary structures and palaeocurrent indicators is interpreted to result from sediment transport in a confined setting, with deflections in the flow (*sensu* Kneller and McCaffrey 1999).
LF11 – Laterally persistent medium- to thick-bedded sandstone (Figure 8)	Fine to very fine (very rarely coarse to medium) grained; medium to thick-bedded (<80 cm)	Pale grey to beige, normally graded, moderate to well sorted sandstone, typically with a relatively coarse grained, lightly scouring base, often with sole marks including flute casts and grooves. Beds are tabular and laterally uniform over tens to hundreds of m across any one outcrop. Lower portions may be massive or planar laminated, grading into finer grained, dewatered horizons and typically capped by current ripples. Rippled intervals may represent more than 50% of the bed and dewatering structures, particularly flame structures, may show a preferred orientation. Laminations often picked out by organic matter.	These sandstones are interpreted as the deposition from low-density turbidity currents (Bouma Ta-b-c). Where rippled to dewatered intervals represent a significant (>50%) of the bed then sustained suspended load fallout and continued bedload transport is inferred (Jobe et al. 2012). Preferred orientations of flame structures indicates continued reworking of sediment by sustained currents, whilst the sediment was dewatering.

		Bioturbation is often present as vertical burrows extending down from overlying mudstones or horizontal traces such as *Scolicia* sp. Bed amalgamations are rare, with thin silt- and mudstones (LF6, 7 or 8) typically separating beds.	
LF12 – Laterally consistent thick to very thick-bedded sandstone (Figures 13–14)	Fine to very fine (very rarely coarse to medium) grained; thick- to very thick-bedded (<31 m)	Pale grey to beige, graded beds of fine to very fine grained, well-sorted sandstone. Bed bases are typically irregular and may truncate underlying strata by up to 10 cm; sole marks, primarily flutes are common. The bases may initially show inverse grain size grading. The lowermost portion (lower 5–10 cm) of beds may show planar lamination, often highlighted by carbonaceous bands, but planar cross-stratification was also observed. Above this beds are typically massive or dewatered. The upper portion may show a return to planar and ripple lamination. This is an idealised succession and beds may show a different order or not all structures. Sole marks, cross-strata and ripples may show subtly different orientations. Beds are typically not amalgamated, with a transition to mudstone of LF7 or rarely directly to LF6; rare trains of internal mud-clasts or grain size breaks may mark amalgamation surfaces. Fragments of plant material up to 10 cm long may show orientation of the long axes. These beds are tabular and may be traced over tens to hundreds of m across any one outcrop.	These beds are interpreted as the deposition from high to low-density, high-concentration turbidity currents (*sensu* Lowe 1982). Massive portions likely deposited under upper stage flow regimes, with high sediment fallout rates, but could have lost structures due to dewatering; both processes indicate rapid deposition. Cross-strata, bed thickness and climbing ripples imply sustained flows. Waning flows may have resulted in the upper portion of beds (Bouma Ta-c). Variation in palaeocurrent indicates transport in a confined setting inducing flow deflections (*sensu* Kneller and McCaffrey 1999). Bed amalgamations, inverse grading of the lower portion and missing fractions imply a proportion of these flows were bypassing and mud-clasts imply these flows had the ability to erode the sea-floor.
LF13 – Laterally inconsistent thick-bedded sandstone (Figure 12A–C)	Fine to very fine (very rarely granular to medium); thick-bedded (<200 cm)	Pale grey to beige irregularly bedded sandstones. Beds typically show a lenticular form, thinning over tens to hundreds of m in width. Bed bases are irregular, with decimetre scale incisions truncating underlying strata. Sole marks, primarily flute casts may scour centimetres into the underlying sediment. Beds variably show planar cross-stratification, extensive dewatering and convolute bedding, grading to planar lamination and ripple lamination at the bed tops or may be massive and contain abundant sand- and mud-clasts. Laminations often highlighted by organic rich bands and carbonaceous debris up to 10 cm long is common. Bed amalgamations are very common. Rarley, beds are granular to medium grained and may have a significant glauconite and bioclastic component. Bioturbation is rare and occurs as large vertical burrows (e.g. *Ophiomorpha* sp.) at bed tops. Macrofossils only observed as broken shell fragments <1 cm.	These lenticular beds are interpreted as the fill of low-aspect ratio scours and/or small channels by deposition from high-density turbidity currents. Bioclastic and glauconitic bed bases implies that at least part of these flows initiated in a shallow marine environment, however the fact that the upper parts of these beds commonly show carbonaceous material and carbonized wood fragments implies some direct terrigenous input.
LF14 – Mud-clast rich sandstone (Figure 12C)	Fine to very fine; thin to thick-bedded (<100 cm)	Pale to medium grey, normally ungraded, sharp based sandstones, typically lacking internal structure, with mud clasts throughout, although often concentrated in local clusters or horizons. Clasts up to 30 cm long, but typically <3 cm. Small clasts typically sub-angular and elongate, becoming more spheroidal and rounded as they increase in size. Typically matrix supported, but beds may rarely be up to 50% clasts. Beds may also be rich in plant debris and or bioclastic fragments. Bioturbation only observed on bed tops.	These mud-clast rich deposits are interpreted as the result of high-density, erosive turbidity currents, entraining semi-lithified mudstones, inferred to be present up-slope. By entrainment of fines, these flows likely lost turbulence and acted as laminar or semi-laminar flows, lacking current structures, but had not yet evolved into hybrid event beds (sensu Haughton et al. 2003).
LF15 – Hybrid event bed (Figure 14E)	Very fine grained matrix with floating mud clasts; medium to thick bedded (<80 cm)	In idealized sections, typically overlying thin (<10 cm), very fine-grained, often rippled horizons of "clean" sandstone (LF10) are medium bedded (20–60 cm) argillaceous sandstones, rich in floating mudstone clasts (up to 60%). Clasts are typically <20 cm long and less than 5 cm thick, sub-spherical and sub-elongate, but become more angular and elongate with reduced size. These are typically overlain by an argillaceous sandstone (LF10), although the overlying sandstone may be truncated by a subsequent bed. Typically matrix supported, which normally consists of a	Interpreted as hybrid event beds, *sensu* Haughton et al. (2003). The basal sandstone represents the head of the flow, which was delaminating the sea floor and entraining mud clasts. This resulted in the body of the flow being deposited as a mud clast rich debrite, over which the tail of the flow deposited a second clean sandstone. This is an idealised succession and all or parts of the event bed may be present.

(*Continued*)

Table 1. Continued.

Lithofacies type	Grain size & bed thickness	Observations	Interpretation
		"dirty" sandstone, rich in micaceous material, organic matter and occasionally bioclasts.	
LF16 – Bioclastic grit (Figures 8E and Figure 11D)	Granular to fine grained; beds up to 100 cm thick, but typically <10 cm	Pale yellow to beige, often weathering orange, beds primarily comprise poorly sorted mixtures of siliciclastic, bioclastic and glauconite grains of variable proportions. Mud-clasts are common, typically <5 cm long, but up to 50 cm. Exotic pebbles are rare. Bed bases typically sharp, erosive and may display scour marks. Beds are variably massive, show coarse laminations or planar cross-stratification. Beds are laterally variable in thickness, grain size and persistence, often seen to pinch and swell. Bioclastic material includes fragments of molluscs, foraminifera, bone material (primarily fish, but also cetacean), corals and other marine organisms. Although rare, terrestrial material, including wood fragments may also be found in these beds. Beds may occur in isolation within mudstones, or more commonly immediately below much finer grained LF9, 10, 11 and 12. Rarely and only in southern localities, these beds may be observed to grade continually from coarse bioclastic material to relatively clean very fine grained sandstones.	These are interpreted because of gravity flows originating from local shallow marine environments, reworking material from marine shelves to deposit them in relatively deep-water. Their common association with very fine-grained material can be interpreted in one of two ways. (1) These beds were triggered simultaneously with finer siliciclastic flows, or (2) They represent a missing grain size fraction in normally graded events. The observation of beds grading normally through medium and fine grain sizes, with decreasing bioclastic content implies the latter was the dominant process.
LF17 – Sigmoidal sandstone (Figure 11A–C)	Fine to very fine grained; beds up to 300 cm thick	Massive, moderately well-sorted sandstones. Bed bases usually sharp but preserve bi-directional ripple casts and/or flute marks. Infrequently basal portion of beds is horizontally laminated. Most beds are structure-less or show dewatering. Signmoidal bedforms are apparent at bed scale, forming foresets as beds amalgamate into packages m to tens of m thick and tens to hundreds of m wide, forming low aspect lenses. Foraminifera of encasing mudstones record mid to upper bathyal water depths of ~700 m.	These sandstones formed in deep and confined settings with currents collecting sand to form the dune like bedforms. The preservation of ripple casts indicates deposits were emplaced progressively without significant erosion of the sea-floor. These bedforms resemble mouth-bar like deposits in a deep-marine setting (see Tinterri 2011 and references within).
LF18 – Shelf siltstone (Figure 15C)	Siltstone; beds typically <500 cm thick	Blue-grey, massive, blocky, thick-bedded siltstones, often amalgamating into packages tens to hundreds of m thick. Bioturbation is moderate, dominated by *Chondrites sp.*, *Glossifungites* sp., *Terebelina sp.* and *Thalassinoïdes sp.*, to pervasive, such that very few burrows are preserved and beds are mottled. Body fossils are rare, including molluscs. Subtle remobilisation may be seen in some large-scale outcrops. Foraminifera record shelfal water depths.	Interpreted as deposition on an outer-shelf. Representing the build-up of background sediment on shelves starved of sediment. Remobilisation indicates local deposition on a periodically unstable angle.
LF19 – Shelf medium to thin-bed (Figure 15B)	Very fine sandstone grading to siltstone; graded beds typically <25 cm	Pale grey, glauconitic, bioclastic, sandstones grading normally to mottled siltstones. Bed bases are sharp, planar to erosive. Wave ripple lamination is sparse; hummocky or swaley cross-stratification is occasionally observed. Flaser and linsen bedding also observed. Bioclastic material is concentrated in thin horizons of shell hash. Extensive bioturbation may give beds a mottled appearance, or large burrows such as *Ophiomorpha* sp. and *Rhizocorallium* sp. Typically grades into or out of intensively bioturbated siltstones (LF18). Foraminifera indicate relatively shallow, shelfal water depths.	These gradational beds are interpreted to reflect the result of storms on a relatively shallow marine (mid-) shelf (Dott and Bourgeois 1982). Storms would have introduced coarser material to the system and concentrated shell debris within tempestite layers (e.g., Hendy et al. 2006), where silt was generally accumulating. Bioturbation may have resulted in destruction of sedimentary structures in some beds.
LF20 – Shoreface to foreshore sandstone (Figure 15)	Fine to very fine grained (rare pebbles of glauconite); beds up to 500 cm thick	Massive, glauconitic, bioclastic, pale blue-grey sandstones. Pervasive bioturbation may give beds a mottled appearance, with *Skolithos sp.*, *Ophiomorpha sp.*, *Palaeophycus* sp., *Teichichnus sp.*, *Thalassinoïdes sp.* seen when bioturbation is weak. Bed bases are sharp, sometimes erosive, and trough cross-bedding or low-angle cross-laminations are sometimes observed; beds are mostly internally structure-less. Beds commonly amalgamate into packages tens of m thick. A wide variety of bivalvia, gastropoda, and scaphopoda as well as less common coral fragments,	These sandstones are interpreted to have accumulated in shallow water, inner shelf areas of the basin and range from foreshore to lower shoreface as demonstrated by the distribution of grain-size, bioturbation, and sedimentary structures (Bailleul et al. 2007). They are found at the basin margin (Bailleul et al. 2013) and during periods of shallowing across the basin. Their stratigraphic occurrence in order with LF18 and 19 imply they are *in-situ*.

		cetacean bones, shark teeth, crab skeletons, and fragments are often concentrated in horizons, as are small sub-angular pebbles of glauconite. Foraminifera record inner shelfal conditions.	
LF21 – Glauconite bed (Figure 15)	Granular to fine grained; beds up to 50 cm thick	Rare occurrences of black (dark green when fresh) beds dominated by glauconite (>90%). Bed bases are sharp and may show centimetre scale erosion, but lack internal structures. The remainder of the bed is typically comprised of bioclastic debris, often with larger molluscs nearly intact, but also with finer shells broken into a hash. Rare pebbles of glauconite occur. They are found in conjunction with deposits interpreted as both shallow and deep-marine, e.g. LF20 and LF13.	These deposits are interpreted to represent storm events reworking authogenic glauconite in low energy marine environment (sensu Amorosi 1995), mixing these with broken shell material and rare exotic clasts. Those associated with deeper water lithofacies may represent down-dip reworking into deep-water.
LF22 – Algal limestone (Figure 15A)	Fine to coarse grained carbonates; beds up to 8 m thick, although typically <50 cm	Cream to pale pink (may weather grey-blue to white) carbonate beds dominantly composed of broken or encrusting red algae, Rotaliida foraminifera and bryozoan fragments, with subordinate broken bivalvia, gastropoda, echinoderms, echinoid spines, benthic and planktonic foraminifers, rare encrusting foraminifera, oyster fragments and scaphopod molluscs; and very rare glauconite and quartz grains. Beds often show sharp, scouring bases and may show a crude stratification, or appear massive, particularly when occurring as laterally discontinuous horizons. Particularly abundant and thickest in southern localities, forming a marker horizon within the Takiritini Fm. (Johansen 1999).	These red algae dominated limestones are interpreted to represent high energy reworking of carbonate factory material in mid to outer shelf settings (Bailleul et al. 2007). Some of these heterozoan carbonate successions consists of forced regressive then transgressive for-algal and rhodolith-bearing deposits (Caron et al. 2021).
LF23 – Densely packed shell beds (Figure 15A)	Large shells and shell fragments highly concentrated, set in a coarse to fine siliciclastic/ bioclastic matrix; beds up to 50 cm thick	Well to very well-cemented, moderately to very poorly sorted skeletal concentrations principally composed of mollusc shells of varying degrees of fragmentation. Although their taphonomic attributes are variable, thicker bivalves such as *Pectinidea, Cucullaeidae*, *Glycymerididae* may be relatively intact, although often disarticulated, whereas thinner shelled specimens are often highly fragmented, forming a significant proportion of the matrix in some beds. Shell diversity is highly variable with some lenticular beds being composed almost exclusively of well-preserved gastropods. Contains subordinate algal, glauconite, and quartz grains. These typically occur as isolated, laterally discontinuous beds associated with LF19, LF20 and LF22.	These are interpreted to represent either high energy reworking of molluscs in inner to mid shelf settings (Bailleul et al. 2007) or deeper starvation on the outer shelf where bioerosion and encrustation is also present. The former includes amalgamated and channelized shell beds and the later are sediment-starved shell beds (Hendy et al. 2006).
LF24 – Moderately to loosely packed shell beds (Figure 15A)	Large shell fragments set in a siltstone to fine sandstone matrix; beds up to 150 cm thick	Well-cemented, bi-modal skeletal concentration comprised of large shells such as bivalvia, gastropoda, scaphopoda, and shell fragments set in a fine carbonate siltstone to fine sandstone matrix. Taphonomic characteristics of shells display a large range from articulated bivalves in living or escape position to highly fragmented molluscs, including thick-shelled specimens, and disarticulated bivalves. Bioerosion and encrustation are absent to low. When very loosely packed, shell beds may show gradational contacts from fine-grained shelf siliciclastics or a gross stratification with shells concentrated at the base when moderately packed.	These shell concentrations may occur as in-situ mid to outer-shelf deposits (Bailleul et al. 2007). The shallow water deposits correspond to rapid-burial, wave/current-winnowed and sediment-dominated shell beds (Hendy et al. 2006).
LF25 – sand injectite	Medium to fine grained; <2 m thick	Massive, well-sorted sandstones, which may show grading towards margins. May occur as small, simple elongate fingers adjacent to sandstones (e.g. LF11 and 13) or as significantly larger sheets and pipes cross-cutting stratigraphy. The host stratigraphy often shows signs of brittle deformation all around these units.	The highly discordant and irregular nature indicates these are injected sandstones. The brittle nature of their associated deformation and the mudstone clasts implies host lithologies were already lithified when the injection occurred.
LF26 – Lignite	Very fine to fine grained; less than 20 cm thick	Very dark brown to black, carbonaceous horizons. No structures, ichnofossils or macrofossils were seen. Represents the rarest lithofacies, occurring in five horizons on the western margin of the uppermost fill of the basin.	These carbonaceous deposits can be classified as an immature coal or lignite.

and the recognition of key lithofacies associations, representative of architectural elements of the basin fill. Biostratigraphic data were provided by GNS Science (Clowes et al. 2021); where not available, samples were collected and analysed by GNS Science to provide new ages. Digital mapping of lithofacies associations in the field, using a Trimble TCD100, were integrated with aerial photographs (LINZ), drone reconnaissance, and supplemented with biostratigraphic information to produce correlations and determine the distribution of architectural elements across the basin.

Data were collected in light of existing stratigraphic information on the basin (Ongley 1935; Kingma 1958; Neef 1967; Johnston 1980; Neef 1981, 1991; Neef and Bottrill 1992; Neef 1992a; 1992b; 1995; 1997; 1999a; 1999b; Bailleul et al. 2007, 2013; McArthur and McCaffrey 2019; McArthur et al. 2021) and used to construct lateral and longitudinal chronostratigraphic charts of the basin fill.

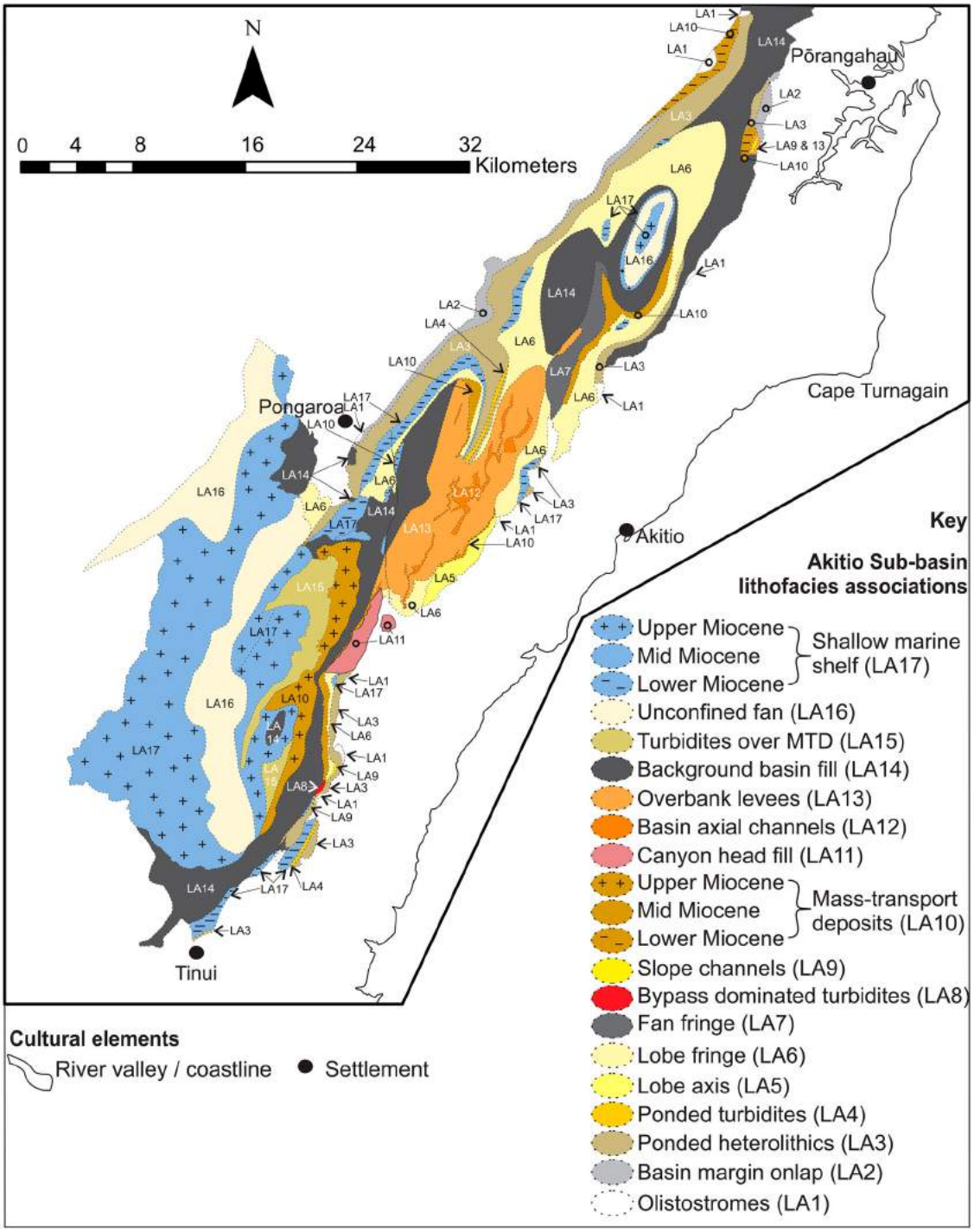

Figure 5. Mapped distribution of lithofacies associations across the Akitio Sub-basin. Largely inferred where exposure is poor. Map suplemented with information from Neef (1992a and 1992b); Neef (1997); Johansen (1999); Lee and Begg (2002); Francis and Johansen (2011) and Heron (2014).

Analogous seismic data of offshore trench-slope basins was provided by WesternGeco and is strictly confidential, hence the precise location of the lines cannot be shown.

Results

Key sections across the basin (Figure 4) allow recognition of lithofacies, lithofacies associations, and are ultimately used to interpret the depositional environment. Associations

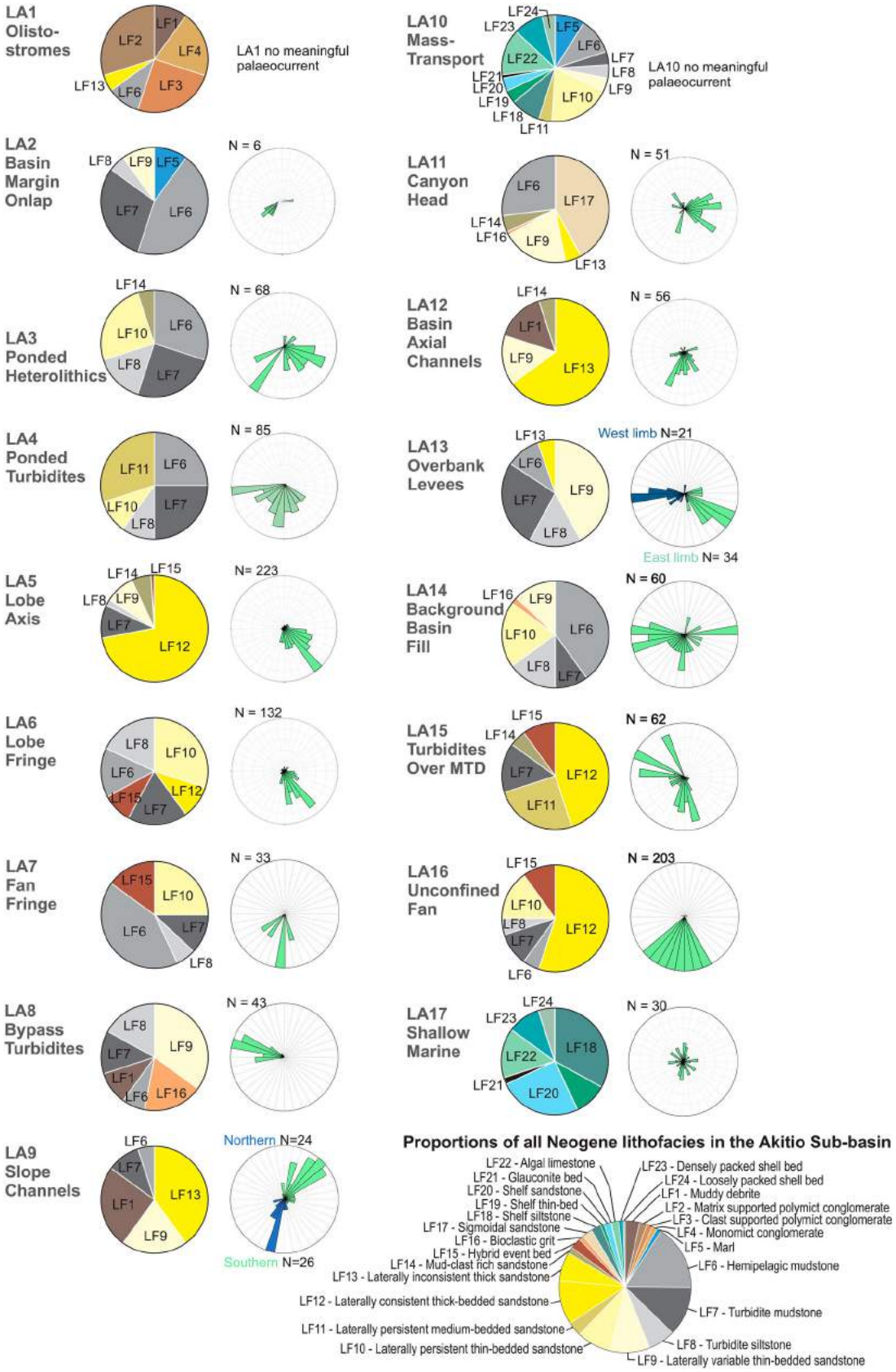

Figure 6. Averaged proportion of lithofacies (LF) in each association (LA) and their palaeocurrent measurements, which were corrected for present day dip.

were mapped across the basin fill (Figure 5) and their composition and palaeocurrents are charted in Figure 6.

Lithofacies

Sedimentary logging allowed the identification of 26 lithofacies, which are described and interpreted in Table 1.

Lithofacies associations

Associations of the lithofacies can be grouped in packages of related sediments to identify lithofacies associations, which may then be interpreted according to their environment of deposition. This interpretation was supplemented by micropalaeontological data. Associations are described in broad order of occurrence in the basin fill, firstly treating deep-water associations and latterly those interpreted as shallow-water deposits. Although treated here for completeness, shallow marine deposits are detailed in Caron et al. (2021).

LA1 – Olistostromes (Figure 7)

Observations: Comprised of matrix (LF2) and clast supported polymict conglomerates (LF3), with rare mudstones (LF1 and LF6), and subordinate thick-bedded lenticular sandstones (LF13) (Figure 7). Clasts are dominantly comprised of older lithologies (e.g. Cretaceous to Paleogene Whangai [Figure 7A and C] or Weber [Figure 7D] formations) and range from pebbles (Figure 7B) to rafts tens of metres long (Figure 7C–D). Rare intraformational clasts also occur, but are typically

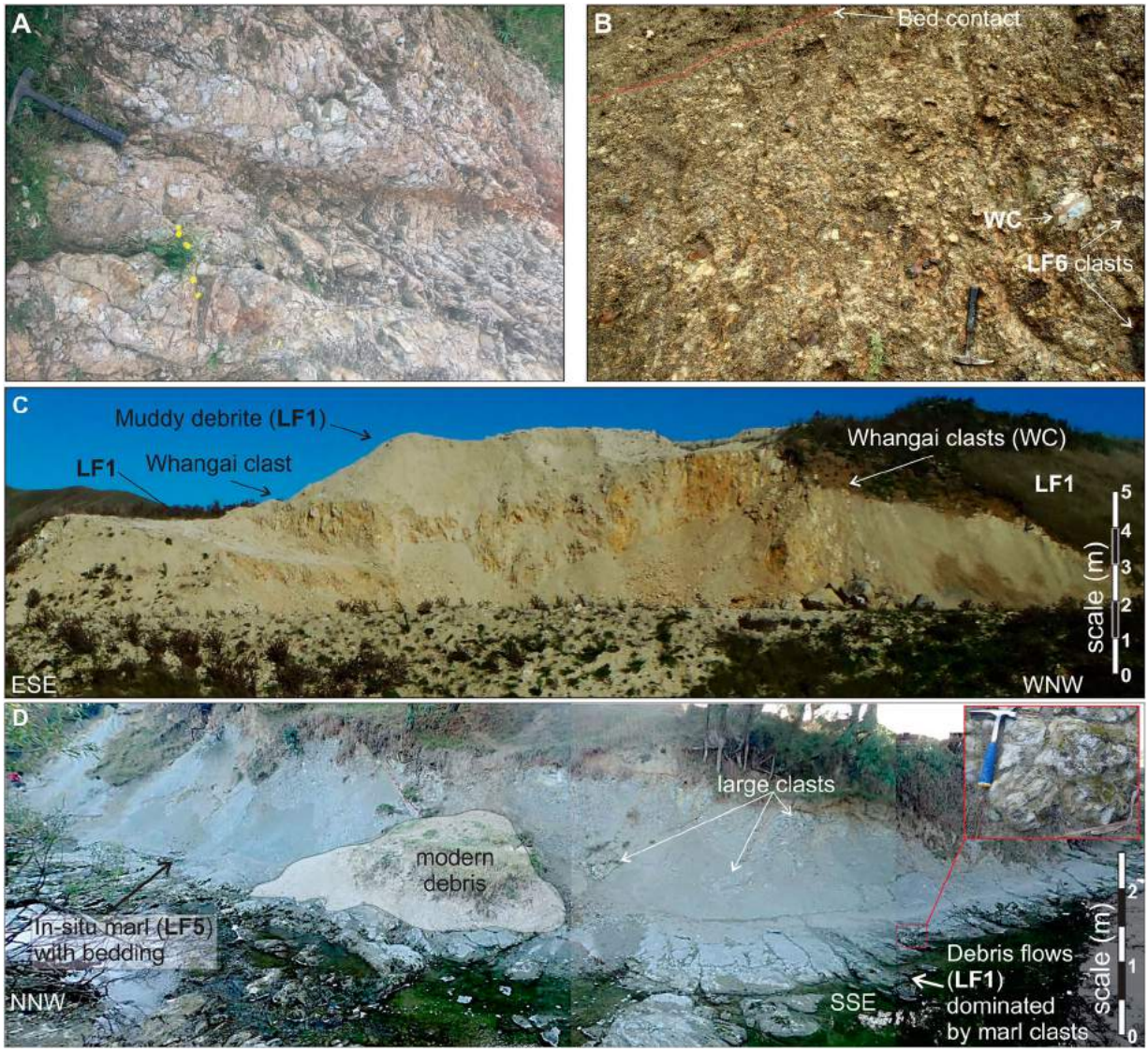

Figure 7. Examples of Lower Miocene mass-wasting deposits on the basin margin. **A,** Clast-supported monomict conglomerates (LF4) comprised of Cretaceous-Paleogene clasts from the Whangai Fm. (WC), with a coarse, dominantly bioclastic matrix at Ugly Hill (−40.203885, 176.639465). **B,** Clast-supported polymict conglomerates (LF3) in Tinui Valley (−40.807509, 176.145792). **C,** Primarily muddy debrites (LF1) but with large Whangai Fm. clasts on the eastern margin of the Akitio Sub-basin at Awapuripuri Station (−40.736605, 176.191193). **D,** Matrix supported debris flow conglomerates principally comprised of marl clasts from the Oligocene Weber Fm. in a muddy matrix (LF2), directly overlying in-situ, bedded Weber Fm. on the western margin of the Akitio Sub-basin near Pongaroa; see inset for detail of clasts (−40.548024, 176.197381). Hammer for scale 35 cm long in all figures.

<5% of any deposit. Some conglomerates may be monomict (LF4) (Figure 7A). These form packages at least tens of metres thick, but given only erosional remnants are preserved they may have formed considerably thicker intervals, as seen in the coastal exposures (Claussmann et al. 2021). This association is found on both margins of the Akitio Sub-basin (Figure 5), such as on the western margin near Pongaroa (Figure 7D) and the northern end of the basin (Figure 5), on the eastern margin near Ware Ware (Figure 4 – base of Coast Road section) and in the Pakowhai River (Figure 4). Similar successions are found at the base of other outcropping basins on the margin (Claussmann et al. 2021). Rare imbrications in conglomerates and traction structures in sandstones indicate transport away from the adjacent basin margin. In places this assemblage is seen to grade laterally and interfinger with Lower Miocene turbidites (Delteil et al. 2006).

Interpretations: This conglomerate-dominated association is interpreted to represent debris flows building slope talus aprons adjacent to the growth structures at the newly formed basin margins. Being found on both the eastern and western basin margin (Figures 4 and 5) implies that the basin-bounding faults had broken to surface early on both margins, to produce the topography required to generate such talus aprons. This association includes the olistostromes of Bailleul et al. (2007), which were interpreted to represent the first effects of subduction on the sedimentary system, forming by erosion of growth structures. Neef (1992a) associated some of these deposits with diapirism, but this interpretation is not preferred given their common occurrence along the margins of the basin. The clasts' composition implies they were primarily sourced from erosion of older strata, likely as it was uplifted in growth structures, but incorporation of intraformational clasts implies the debris flows may have been erosive. Although potentially interpreted as tectonic melanges, interbeddding of such deposits with Miocene aged mudstones and turbidites implies they are sedimentary in nature.

LA2 – Basin margin onlap (Figure 8A)

Observations: A combination of mudstones (LF5, 6, and 7), siltstones (LF8), and thin-bedded, laterally thinning sandstones (LF9), all of which display sporadic remobilisation, primarily in the form of slumps but also larger slide planes, which may incorporate clasts of marl (LF5). Variable palaeocurrents are common (Figure 6), even within the same bed. In rare instances, sandstones are observed to thin and pinch-out against older stratigraphy, particularly in the lowermost basin fill (Figure 8A). Bioturbation is common. Over several to tens of metres this association thickens-up into LA3. Although often deformed by subsequent faulting and poorly preserved due to outcropping on the basin limits, this association is observed at both margins of the basin (Figures 4 and 5) and only in Lower Miocene sections. LA2-4 all contain microfossils indicating deposition in lower bathyal water depths (>1000 m)

Interpretations: This lithofacies association is interpreted to represent onlap of the basin margin by turbidites (*sensu* Kneller and McCaffrey 1999). The variability in palaeocurrents is a result of reflection of flows off a nearby basin margin. Remobilisation may be triggered by a number of factors including fault movements or depositional oversteepening. Thickening of the strata into LA3 is interpreted as a widening of the basin as it was infilled, increasing the distance to the basin margin.

LA3 – Ponded heterolithics (Figure 8A)

Observations: Tabular, thin- to medium-bedded turbidites (LF8 and 10) with significant mudstone caps (LF7), and mudstone interbeds (LF6) are observed to grade up from LA2. Sandstone to mudstone ratio is increased compared to LA2 (Figure 6), but remobilisation is still observed (Figure 8A). As with LA2, a wide variety of traction structures shows variations (Figure 6), which are typically directed southwards in the northern end of the basin and northwards in the southern end. Bioturbation is moderate to intense, but typically concentrated in mudstones. Although preservation and exposures are generally poorer on the eastern basin margin, examples of laterally thinning beds, demonstrating syn-sedimentary deformation are present in the in the Pakowai River section and the Mangarapa section (Figures 4 and 5). This lithofacies typically thickens-up into LA4 and has been observed in the Lower Miocene strata (Figure 4).

Interpretations: This heterolithic association is interpreted as a migration of the depocentre away from the basin margin, likely occurring as the basin filled, therefore driving the onlap margin further from the depositional locus (*sensu* Kneller and McCaffrey 1999). This implies that these thin- to medium-beds were ponded within the basin (e.g. Marini et al. 2016). The variety of palaeocurrents indicates that multiple sediment input points existed during deposition. As with the debris flow deposits (LA1) that they are often found adjacent to, the presence of this association on both eastern and western margins implies that both basin margins presented topography shortly after the formation of the basin.

LA4 – Ponded turbidites (Figure 8B)

Observations: Tabular, medium- to thick-beds (LF11) and thin-beds (LF10) with significant turbidite mud-caps (LF7 and 8), and rare hemipelagic (LF6) mudstone interbeds, observed to grade up from the thinner bedded LA2-3. Sandstones typically show significant traction structures, with climbing ripples and or sheared flame structures often representing >50% of the beds. Mud-caps are typically at least as thick as the underlying sandstone (Figure 8B). Bioturbation

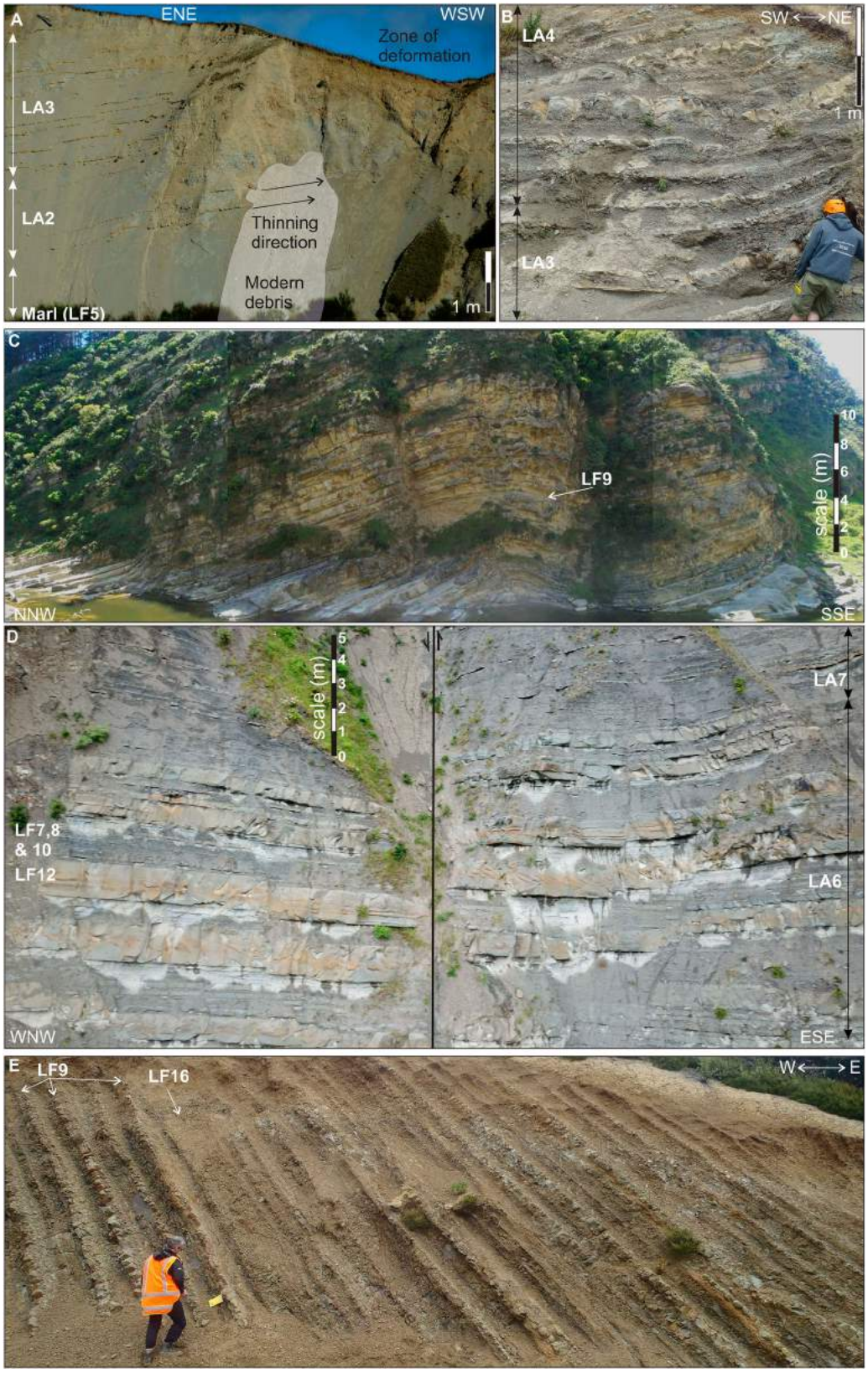

Figure 8. Lower Miocene basin fill lithofacies associations. **A,** Basin margin onlap (LA2) grading into ponded heterolithics (LA3), both comprised of alternating turbidites (LF7-10) and hemipelagic mudstone (LF6) on the western margin of the Akitio Sub-basin (−40.449780, 176.290819). **B,** Ponded turbidites (LA4) close to Pongaroa (−40.548654, 176.198867). **C,** Lobe axis (LA5) in the Owahanga Gorge (−40.629484, 176.273351). **D,** Lobe fringe (LA6) and fan fringe (LA7) at the Pongaroa Gun Club (−40.558760, 176.225753). **E,** Bypass dominated thin-bedded turbidites and grits (LA8) on the Tinui Valley Road (−40.771628, 176.168920), with person for scale.

is moderate to intense across all lithofacies. This association has been observed in the Lower Miocene succession of the basin (Figure 4). As with LA3, sole marks may show offset palaeocurrents to overlying sedimentary structures, but again suggest multiple pathways in the basin (Figure 6).

Interpretations: This dominantly thick-bedded association, where mud-caps are typically at least as thick as the sandstones deposited by sustained flows, are interpreted as turbidites ponding in depocentres. The thickness of the mud-caps implies that the suspension clouds of turbidity were contained, as well as the coarser grade of the flows (Patacci et al. 2015).

LA5 – Lobe axis (Figure 8C)

Observations: Tabular, thick-bedded, normally amalgamated and dewatered sandstones (LF12), with rare turbidite silt- to mudstone-caps (LF7 and 8), irregular thin-beds (LF9), mud-clast rich intervals (LF14), and hybrid event beds (LF15). For a detailed description see McArthur et al. (2021). This association is often amalgamated into packages tens to hundreds of metres thick (Figure 8C), reaching over 200 m in thickness of stacked, high net to gross (N:G) deposits in the Owahanga Gorge (Figure 5). Sandstones often show internal scours, grain-size breaks, and discrete gravel lags (LF16) within sole marks. Bioturbation is typically restricted to mud-caps and includes large burrows such as *Ophiomorpha* sp. and *Thalassinoides* sp. This association occurs in the Lower Miocene strata, where sole marks and other sedimentary structures are typically aligned, generally showing a SE direction (Figure 6). Foraminiferal associations indicate deposition in water depths >700 m.

Interpretations: These laterally extensive, sandstone-dominated deposits are interpreted as axial deposits of deep-marine lobes (McArthur et al. 2021). Lack of, or very thin mud-caps implies that a significant proportion of the flows were not being deposited here, but were bypassing down-stream. The aggradational stacking patterns observed implies the deposits were confined by the growing basin structure, pinning deposition in the same location. Palaeoflow to the SE was towards the NE-SW aligned basin edge (Figure 3), which was likely less than 2 km away during deposition (Bailleul et al. 2013).

LA6 – Lobe fringe (Figure 8D)

Observations: Laterally continuous thin-beds (LF10) with sporadic tabular thick-beds (LF12), separated by turbidite and hemipelagic mudstones (LF7-6), siltstone (LF8) and hybrid event beds (LF15), occurring in packages tens to hundreds of metres thick (Figure 8D). These may be seen to grade out of LA4 or occur in isolation across the Lower Miocene basin fill (Figure 5). Bioturbation is common across all lithofacies. Sole marks and sedimentary structures higher in the beds exhibit similar palaeocurrent directions (Figure 6).

Interpretations: These laterally extensive, sandstone-rich deposits are interpreted as lobe fringes (McArthur et al. 2021). The decreased sand content, presence of hybrid beds, and association with LA5 imply these form the margins of a lobe system (e.g. Kane et al. 2016). Despite showing thick-mud caps, these differ from the ponded turbidites (LA4) in that beds show fewer traction-structures, do not show palaeocurrent deflections, and have a wider variety of bed thicknesses (Figure 8B and D).

LA7 – Fan fringe (Figure 8D)

Observations: Laterally continuous thin-beds (LF10) and subordinate hybrid event beds (LF15), with thin turbidite silt- and mudstone-caps (LF7-8) separated by hemipelagic mudstones (LF6), often at least as thick as the underlying turbidite. This association displays a low N:G and may be seen to grade from LA6 or occur as isolated packages tens to hundreds of metres thick (Figure 8D). Bioturbation is typically sparse, as are structures within the sandstones. This association occurs across in the northern end of the basin in Lower Miocene strata (Figure 5).

Interpretations: Marginal deposits to a larger turbidite system. These sporadic thin-beds and hybrid event beds, interbedded with significant proportions of hemipelagic mudstone are interpreted to represent the fringe deposits to the LA5-6 submarine fan (Prelat et al. 2009). They can be differentiated from LA6 by the absence of thick-beds and lower sandstone content.

LA8 – Bypass dominated thin-bedded turbidites (Figure 8E)

Observations: Irregular thin- to medium-beds (LF9), occasionally underlain by bioclastic grits (LF16), often directly overlain by very thin hemipelagic mudstone-caps (LF6), and accompanied by muddy debrites (LF1) (Figure 8E). They typically show a significant degree of scour, which can be filled with siltstone (LF8) or mudstone (LF6-7). Bioturbation is typically limited to large vertical burrows, e.g. *Ophiomorpha* sp. These occur in association with the Lower Miocene LA5-6 and Middle Miocene LA9 and LA11. In the central to northern portion of the basin, north of the Three Kings Ridge (K in Figure 3) there is a sharp grain size break within beds from the typically coarse basal grit to fine siliciclastic sandstone; in the southern end of the basin the grits grade normally into the overlying siliciclastic interval.

Interpretations: These irregular thin-beds are interpreted to represent fill of scours on the seafloor. Scours are variably filled by deposits of low-density turbidity currents or even directly by hemipelagic mudstones, implying flows that created the scours were not depositing a significant portion of their load as they passed. Therefore, these beds characterise bypass-dominated areas of the basin; flows may have been bypassing to other areas of the same basin, or escaping into other basins via spill points (McArthur and McCaffrey 2019). The coarse bioclastic grits associated with these events are another indicator of bypass, typically being sharply overlain by much finer grained sandstone, implying a missing grain size fraction, inferred to have bypassed down-stream.

LA9 – Slope channel complexes (Figure 9)

Figure 9. Examples of slope channel fills (LA9). **A,** Lower Miocene channel fills in the northern end of the basin (−40.349171, 176.520484). **B,** Irregular thin-bedded turbidites (LF9) and hemipelagic drapes (LF6) of scours within LA9 (same locality). **C,** Base of an LF13 bed showing flute marks in a channel fill in the southern end of the basin (−40.943666, 176.087065). **D,** Sand-rich channel fill in the southern end of the basin, dominated by LF13; with minor LF1 (−40.774862, 176.172366). **E,** Channel fill in the southern end of the basin, dominated by LF13 and LF1 (−40.944072, 176.086691).

Observations: Lenticular packages of heterolithic sediment, typically comprising thick (LF13) and thin-bedded sandstones (LF9), and subordinate mudstones (LF1) and (LF6) (Figure 6), into which they incise and are commonly overlain (Figure 9A). They occur in discrete intervals in packages up to 20 m thick and <300 m wide. A vertical and lateral offset stacking of lenses is apparent (Figure 9A). This Lower Miocene association has been observed in both the northern (Figure 9A–B) and southern (Figure 9C–E) regions of the basin (Figure 5); in the north they exhibit a SSW palaeoflow and vice versa in the south (Figure 6).

Interpretations: These isolated lenses are interpreted as the fill of bypass-dominated slope channels (e.g. Galloway 1998). The variety of often fine-grained

Figure 10. Mass-transport and associated lithofacies associations (LA10). **A,** Basal Middle Miocene mass-transport deposit (MTD) composed of a mudstone matrix, with shallow and deep-marine clasts in a tributary to the Waiowaka Stream (−40.575844, 176.227140). **B,** A small part of a major Upper Miocene MTD comprised of remobilised thin-bedded turbidites exposed in the Pakowhai River (−40.699870, 176.159286). **C,** Small scale Lower Miocene MTD displaying slump folds in thin-bedded turbidites near Mt. Attila (−40.579679, 176.286893). **D,** Disaggregated Upper Miocene MTD, largely composed of mudstones, but with floating sandstone clasts on the Waihoki Valley Road (−40.643657, 176.099938).

fill implies these were bypass dominated for much of their lifespan. These were more than likely the conduits supplying sediment deposited within the basin centre (i.e. LA2-8); modern equivalents can be seen on the present day seafloor (Crisóstomo-Figueroa et al. 2020).

LA10 – Mass-transport deposits (MTDs) (Figure 10)

Observations: Comprising chaotic and deformed packages of a variety of intrabasinal lithofacies, primarily either LF5-11 or LF18-24 in packages up to 150 m thick (Figure 10A). Rafts of other lithofacies associations, metres to tens of metres thick and tens to hundreds of metres long, may form jumbled packages (Figure 10B). Deformation is variable but includes shearing of basal surfaces and internal fracturing, minor to major slump folding (Figure 10C), to almost complete disaggregation with a transition towards muddy debrites (LF1; Figure 10D), containing coherent clasts tens to hundreds of metres long of other lithofacies. Rafts are generally internally coherent and good quality outcrops are required to identify their often-subtle juxtaposition. Careful measurement of bedding orientations between shear zones may also help to distinguish these from in-situ strata. The matrix invariably comprises silty mudstones. Folding or contortions of strata may occur, but other structures or bioturbation are not observed. This assemblage occurs sporadically throughout the basin fill, but major deposits mark the base of the Middle Miocene, being largely composed of remobilised shallow marine facies, and the base of the Upper Miocene, which is composed of remobilised turbidites (Figure 4); these deposits can be traced across wide areas of the preserved basin fill (Figure 5).

Interpretations: Remobilisation of intrabasinal material with rafts set within a siliciclastic matrix are interpreted as mass-transport deposits, which range from metres to seismic scale in thickness and distribution. These deposits typically show extensive deformation of strata and can be interpreted as slumps, but also include competent rafts that can be described as slides. They exclusively remobilised syn-subduction basin fill, rather than pre-subduction material (see LA1). That rafts are coherent implies a degree of burial and compaction prior to remobilisation. Occasionally the sense of transport may be inferred by slump fold orientation or shear direction. The widespread occurrence of these deposits indicates that they filled or partially filled basins, as can be observed in modern offshore basins, such as the Poverty Re-entrant (Mountjoy and Micallef 2012). Although tectonic deformation is also apparent, the presence of these units within intervals of coherent strata, presence of syn-sedimentary features (i.e. slumps), and lack of associated tectonic fabrics implies the described units are sedimentary in nature.

LA11 – Submarine canyon fill (Figure 11)

Observations: Association dominated by sigmoidal sandstones (LF17), interbedded with laterally inconsistent thick-bedded sandstones (LF13), laterally variable thin- to medium-bedded sandstones (LF9), bioclastic grits (LF16), and mud-clast rich sandstones (LF14). The base of this association occurs as a wide (~7 km) and deep scour (430 m) into underlying strata (Figure 4). The associated sediments coalesce into 14 laterally and vertically offset stacked packages each up to 3 km wide and tens of metres thick. A variety of palaeocurrents was recorded, but they are dominantly eastward (Figure 6). This association only occurs on the preserved eastern margin of the Akitio Sub-basin, where it forms the Three Kings Flat Irons (Figure 11A–B). Palaeocurrents from contemporaneous associations, such as LA12 appear to converge upon this area (Figure 6).

Interpretations: These deposits were interpreted as the fill of a deep-marine canyon head by McArthur and McCaffrey (2019), which had incised the Coastal Block and acted as a bypass conduit to downstream basins. Analysis of foraminifera recovered from bounding mudstones indicates a middle bathyal (~700 m) water depth and provides a Langhian age, which corresponds to an angular unconformity recognised across much of the basin (Bailleul et al. 2013). This implies that a phase of significant bypass occurred in association with the canyon cut, with this area representing a major spill point from the basin.

LA12 – Basin-axial channel complexes (Figure 12A–C)

Observations: Thick-bedded, lenticular sandstones (LF13 and 14), exhibiting a relatively low aspect ratio with frequent amalgamation into packages up to 15 m thick and up to 1 km wide (Figure 12A). Individual sandstone packages often stack in the same locality but are typically separated by irregular thin-beds (LF9). As a whole, this association is seen incising various substrates including thin-beds (LF10), mudstones (LF6), MTDs (LA10), and it is laterally bound by LA13. Rarely, muddy debrites (LF1) are seen at the base (Figure 12B). Sandstones often show stepped incision surfaces and internal structures primarily as low angle cross-stratification (Figure 12C). Bioturbation is typically moderate in sandstones to intense in mudstones. This association has primarily been observed in the central portion of the Middle Miocene basin fill and referred to as the Benvorlich Member by Neef (1992b). However, multiple units were since mapped, all of which show a north–south orientation; sole marks indicate flow towards the south (Figure 6). These have been mapped across the crest of the major intra-basinal Kawakawa Anticline (Figure 3).

Interpretations: These low aspect ratios, often vertically stacked, aggradational sandstones are interpreted as the fill of shallow but relatively wide channels following the basin axis (e.g. Hubbard et al. 2008). The presence of bypass thin-beds between sandstones may imply that the actual depth of channel cuts was significantly deeper than the preserved sandstone thickness, even before compaction; this may also account for the abnormally low aspect ratio, often in the range of 100:1. The fact that these channels are

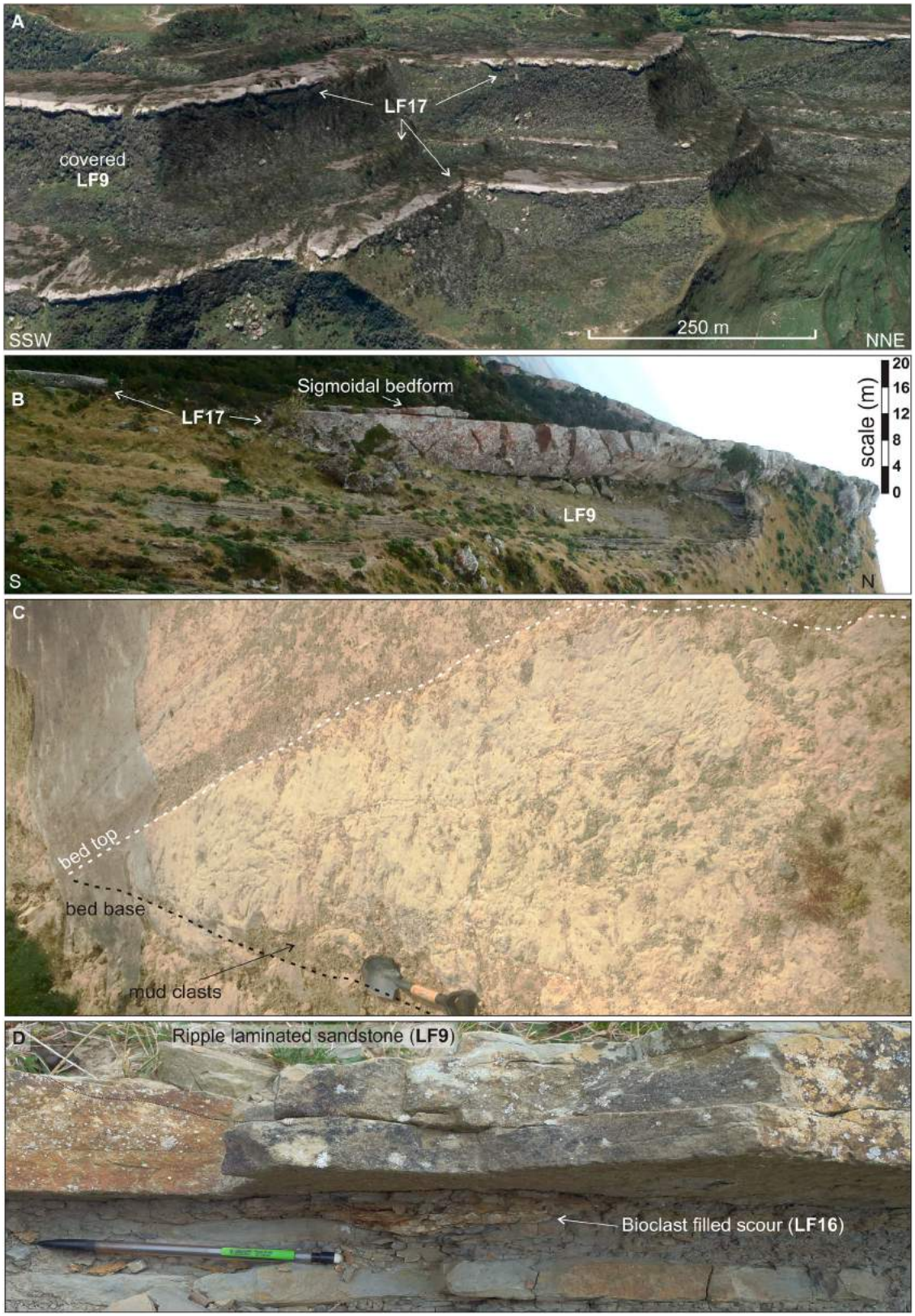

Figure 11. Submarine canyon head fill (LA11). **A,** Aerial photograph imagery (courtesy of LINZ) draped over a digital elevation model over the Three Kings area, demonstrating the large-scale lenticular nature of the sigmoidal sandstone bodies (LF17). **B,** Canyon head lithofacies association on the eastern margin of the Akitio Sub-basin (−40.668029, 176.207717). **C,** Detail of a sigmoidal sandstone (LF17) pinching out, with mud clasts concentrated at the base (−40.670556, 176.219444). **D,** Detail of irregular thin-bedded turbidites (LF9 & 16) in the canyon head (−40.669007, 176.208715).

mostly filled with fine-grained sandstones and bypass related thin-beds implies that a large portion of the flows that carved these channels were bypassed and no terminal sites of deposition are associated with these channels. That they generally trend due south implies they are connected to a spill point (LA11). Mapping of channels across the crest of the intra-basinal Kawakawa Anticline implies that this structure did

Figure 12. Middle Miocene lithofacies associations. **A,** Basin axial channel complex (LA12), showing a thicker overlying channel fill and a thinner underlying channel fill (LF13) separated by irregular thin-bedded turbidites (LF9) in the centre of the basin (−40.545494, 176. 308672). **B,** Detail of the base of the overlying channel fill, showing a basal mudstone debrite (LF1) with clasts of mudstone and sandstone (same locality). **C,** Detail of an incision surface within LF13, showing a sandstone filled channel incising an earlier sand- and mudstone-filled channel (same locality). **D,** Deformed overbank levees (LA13) in the centre of the Akitio Sub-basin (−40.603071, 176.279977), showing multiple stages of failure and healing and a sand-rich lens (LF13) interpreted as a crevasse splay fill. **E,** Background basin fill thin-bedded turbidites (LA14) in the Akitio Sub-basin (−40.660125, 176.194133).

not have a presence on the seafloor in the Middle Miocene, as channels would likely have been deflected by such structures (Clark and Cartwright 2012).

LA13 – Overbank levees (Figure 12D)

Observations: Thin-bedded, laterally thinning, although rarely observed to completely pinch out,

turbidites (LF9, subordinate LF8) with medium to thick turbidite mudstones (LF7), heavily bioturbated hemipelagic mudstone caps (LF6), and rare, isolated lenses up to 10 m wide of thick sandstones (LF13). This association often stacks into packages tens to hundreds of metres thick. Sandstones typically show a range of traction structures exhibiting palaeocurrents oblique to those of adjacent channel fills (Figure 6). Remobilisation and disruption is common, recognised as slide scars, rotated blocks, and slumps (Figure 12D). These deposits are typically found within two kilometres lateral to LA12 (Figure 5).

Interpretations: These laterally variable and often remobilised thin-beds, which occur adjacent to channel fills are interpreted as levees (*sensu* Kane and Hodgson 2011). The remobilisation, subsequent healing, and aggradation implies repeated incision, collapse, and regrowth of this association. The compound thickness, being hundreds of metres, implies channels were larger than their preserved fills. Furthermore, to build levees of this scale implies that substantial amounts of material must have passed through the parental channels. Small sandstone lenses representing scour fills within these intervals are inferred to be deposits of crevasse splays (Posamentier 2003).

LA14 – Background basin fill (Figure 12E)

Observations: Dominantly comprised of hemipelagic mudstones (LF6), with subordinate, sporadic but laterally continuous silt- (LF8) or sandstone turbidites (LF10), and bioclastic grits (LF16). Hemipelagic mudstone commonly accounts for >40% of these intervals, which shows bioturbation particularly in the turbidite component. Palaeocurrents are normally uni-directional in any section, but rare scours may be filled with irregular thin- to medium-bedded sandstones (LF9); generally palaeocurrents are variable across the basin (Figure 6). Large-scale remobilisation is often subtly displayed in the form of discrete slide scars, particularly located in thicker mudstones. This may occur as isolated intervals metres to tens of metres thick, or as major intervals up to ~750 m thick in the Middle Miocene of the basin (Figure 5).

Interpretations: This hemipelagite dominated association provides an indicator that the area of the basin these were deposited in was relatively starved of sediment. This is not to say the whole basin was starved, with this association following the channel-levee system of LA12-13. This association represents the Tanawa Formation of Neef (1992a).

LA15 – Turbidites filling topography on top of MTDs (Figure 13)

Observations: This association comprises laterally persistent turbidites that are highly variable in thickness (LF12) directly overlying major MTDs (LA10). The first sandstone overlying the MTD can be tens of metres in thickness, with amalgamation, but thins rapidly over tens of metres laterally to sub-metre thickness or complete absence (Figure 13A–C). For example, Neef (1992b) recognised that the basal Upper Miocene Pakowhai Sandstone changes thickness from 0 to 15 m over several kilometres (Figure 4). These sandstones are typically overlain by a series of relatively thinner, medium to thick-beds (LF11) with significant mudstone caps (LF7), together with hybrid beds (LF15) (Figure 13D). Basal beds are typically structureless or dewatered, whilst the relatively thinner overlying beds may show a range of traction structures, with palaeocurrents within and between beds often variable (Figure 6).

Interpretations: This association of very-thick to thick-bedded sandstones, is interpreted to represent turbidites filling topography on top of MTDs (Kneller et al. 2016). These deposits are sand-rich, but their distribution is sporadic and dependant on relic bathymetry created by the MTD. That significant mud-caps overly most sandstones indicates that parts or all of the flows were being contained, indicating that significant topography must have been generated by the MTD, at least enough to contain the majority of the turbidity current.

LA16 – Unconfined submarine fan (Figure 14)

Observations: This association is dominated by very-thick sandstones (LF12), interbedded with fines (LF6-8), thin-bedded turbidites (LF10), and hybrid beds (LF15). These show a progression from north to south, with southward palaeocurrents (Figure 6). In the north of the basin (Mt. McCartie, Mc in Figure 3), sandstones are amalgamated into beds up to 31 m thick, show significant scour, and mud-clast rich intervals but no hybrid beds (Figure 5; 14A and B). In the intermediate portion of the basin (Mangatiti – Waihoki Valley, M and W Figure 3), the turbidites are dominantly thick-bedded, but demonstrate less amalgamation, with beds typically 1-5 m thick and separated by siltstones and hybrid beds (Figure 14C). To the south (Annedale, A in Figure 3), sandstones are rarely amalgamated and the proportion of hybrid beds is increased (Figure 14D and E). Siltstones bounding these deposits are typically blocky, heavily bioturbated and with foraminifera recording relatively shallow water depths, (upper bathyal; 400–600 m) and a latest Miocene age.

Interpretations: These deposits are interpreted as a relatively unconfined submarine fan prograding along the basin axis, filling residual depocentres, with a progressively distal expression downstream, towards the hybrid bed rich terminal region (*sensu* Kane et al. 2016). Although only outliers are preserved, the inference is that by the end of the Miocene the basin had been mostly infilled, but still presented a subtle relief to orientate the deposits along the basin axis.

LA17 – Shallow marine shelves (Figure 15)

Observations: Broad cycles are often apparent within these strata, grading out of underlying deep-marine sediments, sometimes over an angular

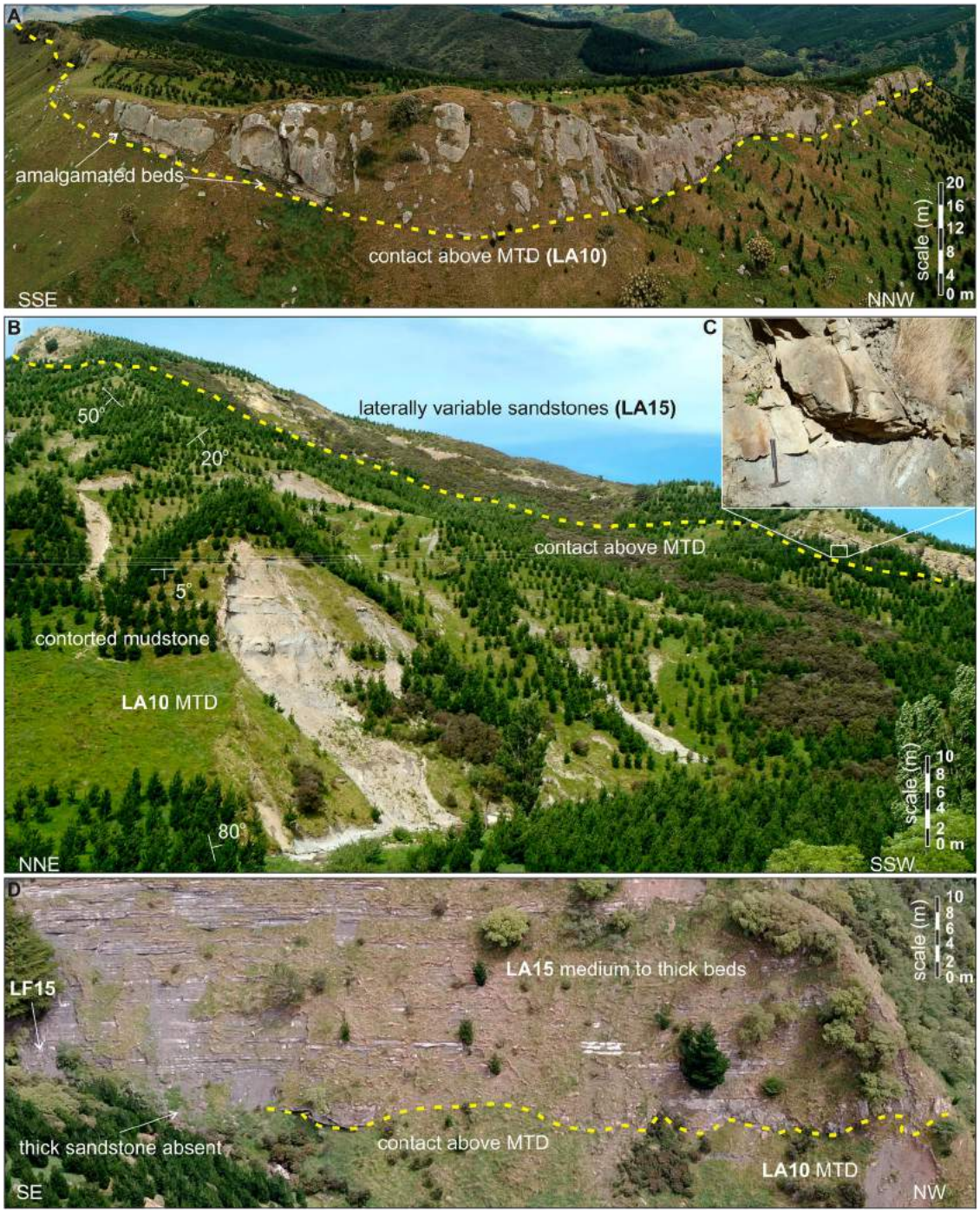

Figure 13. Examples of LA15 strata overlying the major MTD (LA10) that marks the base of the Upper Miocene basin fill. **A,** Overview of the thick basal sandstone (LF12) immediately overlying the MTD; note evidence of bed amalgamation (−40.624775, 176.184797). **B,** Wider view of the underlying MTD, showing various dip angle and direction and the overlying thick sandstone (LF12), which shows significant thickness variation along strike (−40.621538, 176.170715). **C,** Close up view of the basal contact, showing irregular clasts in the underlying MTD and scouring, fluted base to the thick sandstone (LF12). **D,** The basal sandstone (LF12) varies from being absent, to thickening markedly over the MTD topography. Overlying beds (LF11-12) show more uniform thickness and presence of hybrid event beds (LF15) (−40.621771, 176.169066).

unconformity (D4 and 6; Figure 4), into a series of bioturbated siltstones (LF18; Figure 15C), laterally persistent very-thick bedded, sandstones (LF20-21; Figure 15B), intercalated with thin-beds (LF19), punctuated by shell beds (LF23-24). Locally they are capped by limestone (LF22; Figure 15A) and ultimately by drowning surfaces, before resumption of deep-water strata deposition. This association may be isolated and thin, < 10 m thick, particularly on the eastern edge of the basin, ranging up to 800 m thick in the southernmost end of the basin (Johansen 1999). In the uppermost basin fill rare horizons of lignite are present (LF26). On a large scale, outcrops occasionally exhibit large scale clinoforms, however sediments are generally massive, rarely display traction but not turbulent structures, e.g. flaser bedding, being dominated by

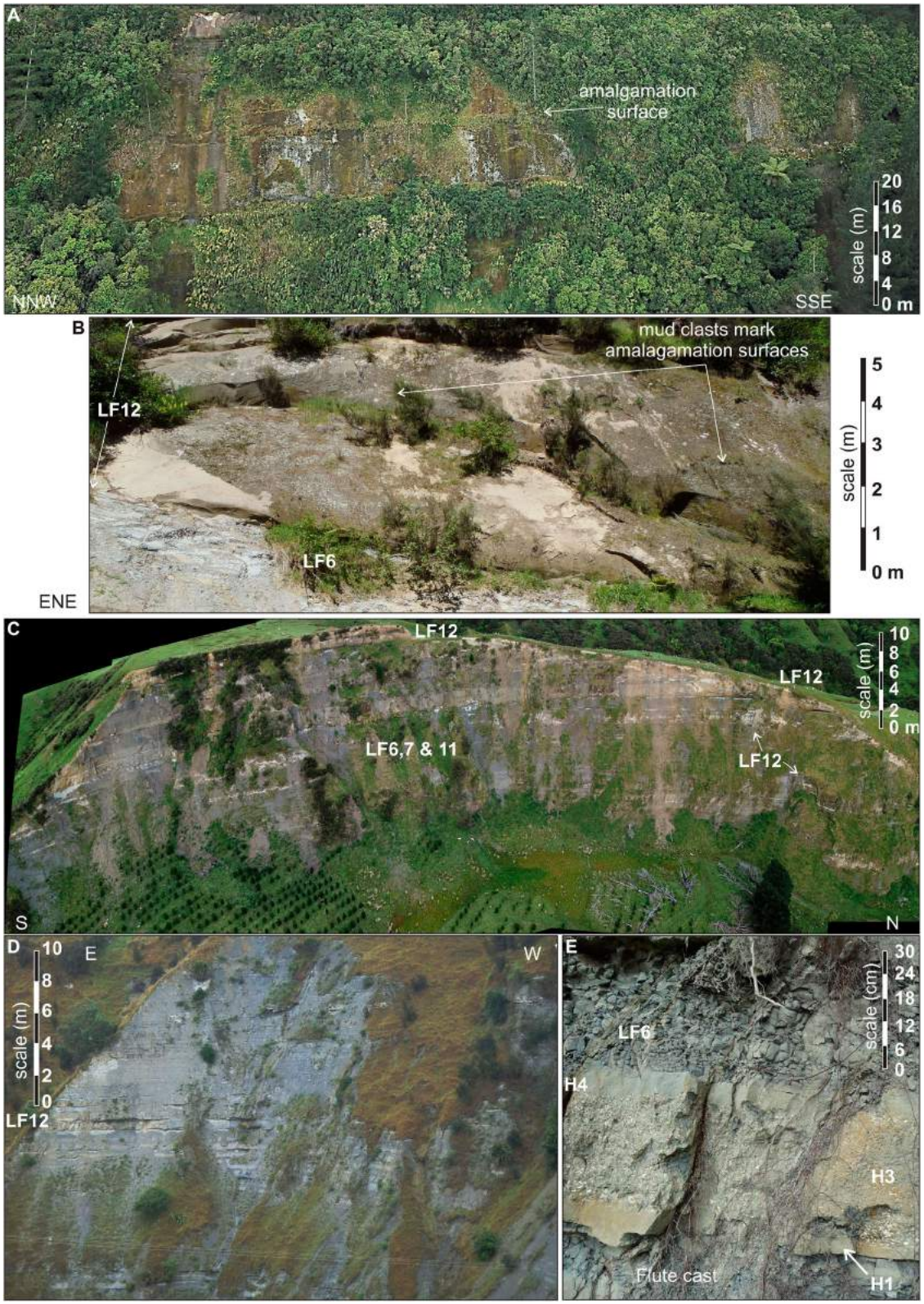

Figure 14. Character of unconfined Upper Miocene submarine fan (LA16) across the basin. **A,** At Mt. McCartie, in the northern end of the basin, where sandstone beds may amalgamate up to 31 m in thickness (−40.427461, 176.420507). **B,** Detail of the base of the 31 m thick sandstones, showing multiple discrete amalgamation surfaces, some picked out by mud-clast horizons (−40.403487, 176.438319). **C,** ~33 km further south, sections on Rimu Road demonstrate very thick (up to 5 m thick sandstones), but less amalgamated beds (−40.585853, 176.083856). **D,** A further 18 km south beds of the same age are mostly medium- to thick-bedded (LF11), other than the labelled thick–beds (LF12) and show no amalgamation (−40.748040, 176.077974). **E,** Hybrid event beds (LF15) become a common component of the strata (same location); H divisions after Haughton et al. (2003).

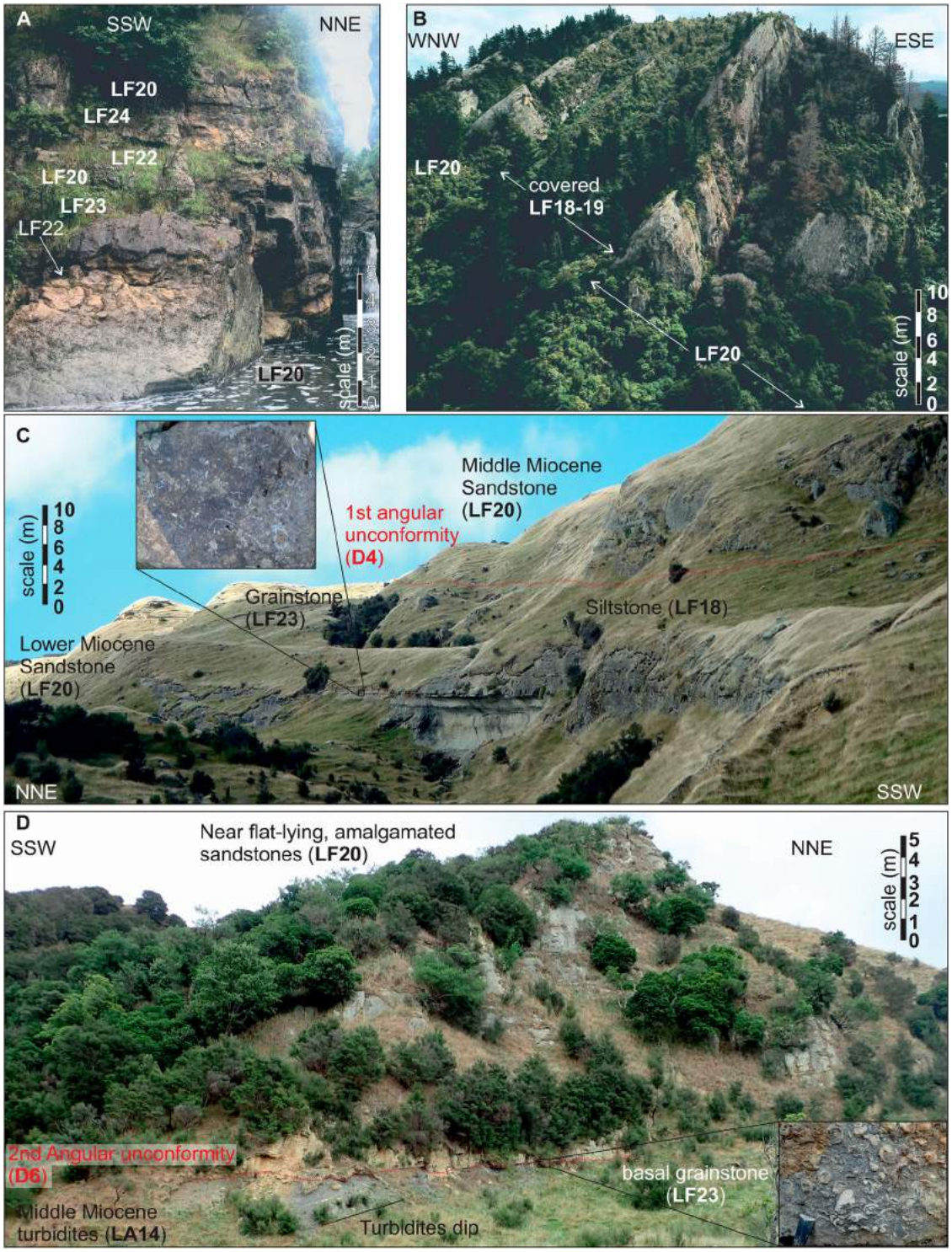

Figure 15. Shallow marine lithofacies associations (LA17). **A,** Alternating sandstone and carbonates in Lower Miocene shallow marine deposits at the southern end of the basin (−40.809271, 176.155972). **B,** Sand-rich Lower Miocene shallow-water succession at Maunsell Trig (−40.863404, 176.086417). **C,** Lower and Middle Miocene shelf deposits separated by an angular unconformity (AU1) at Waihoki Trig (−40.610016, 176.172785). **D,** Upper Miocene shelf deposits resting on an angular unconformity (AU2) over Middle Miocene strata in Glenross Gorge (−40.579526, 176.133729).

oscillatory fair- or storm-weather structures. Analysis of macro and miocrofaunas indicate deposition was dominantly in inner to outer-shelf conditions, c.a. <200 m water depth (Bailleul et al. 2013).

Interpretations: These strata have previously been described under a variety of names and ages, e.g. the Lower Miocene Takiritini Fm. (Johnston 1980) and Coast Road Fm. (Neef 1992b), the Middle and Upper Miocene Ngarata Sandstone (Neef 1992b), and the shelf deposits of Bailleul et al. (2007; 2013). These sediments are interpreted to have been deposited under shallow marine conditions, with a spectrum from foreshore to outer shelf depositional settings on shelves developed on the flanking structural highs, which occasionally prograded into the basin. They typically demonstrate a gradation from siltstones (LF18) to

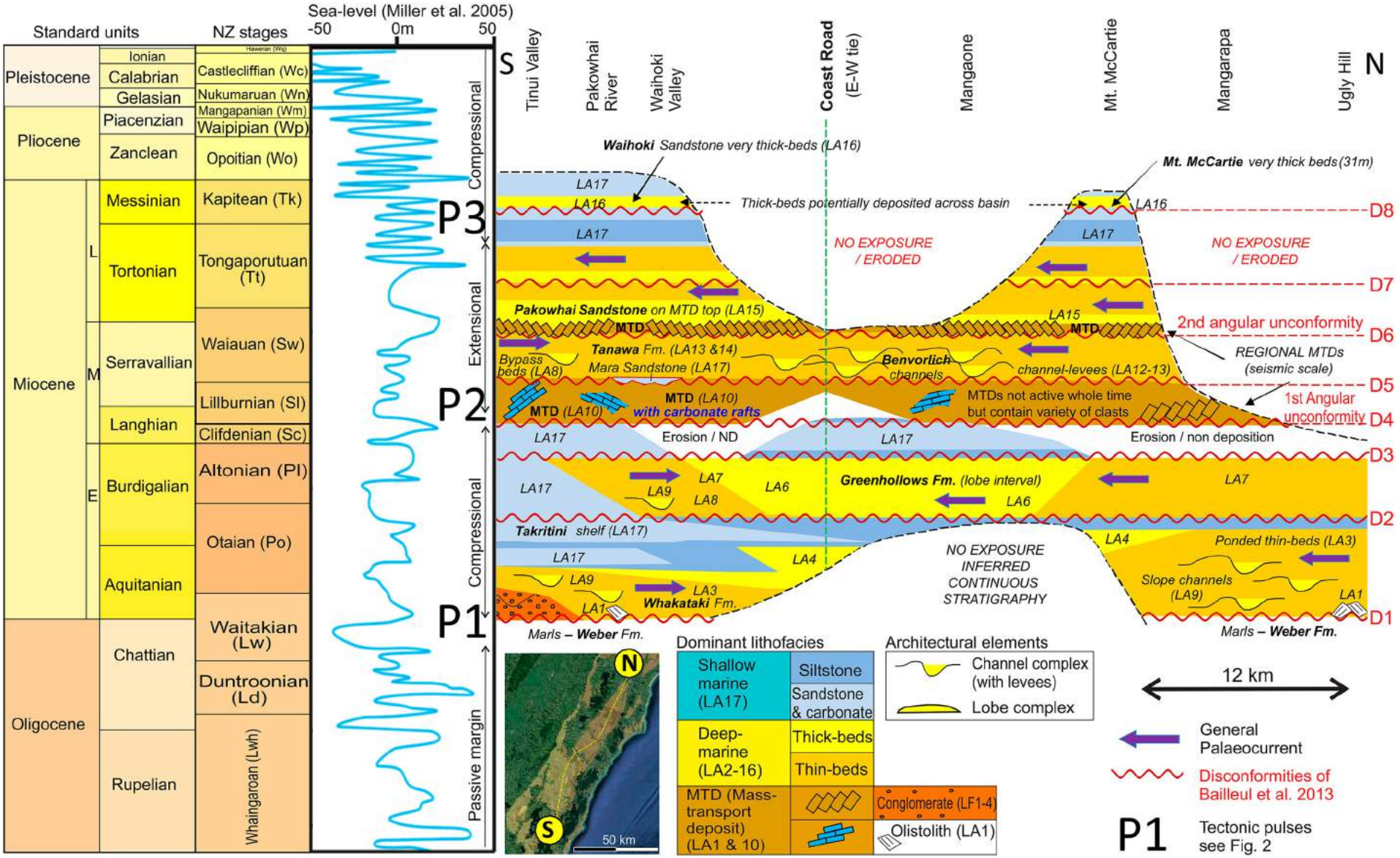

Figure 16. Chronostratigraphic chart from north to south along the basin axis.

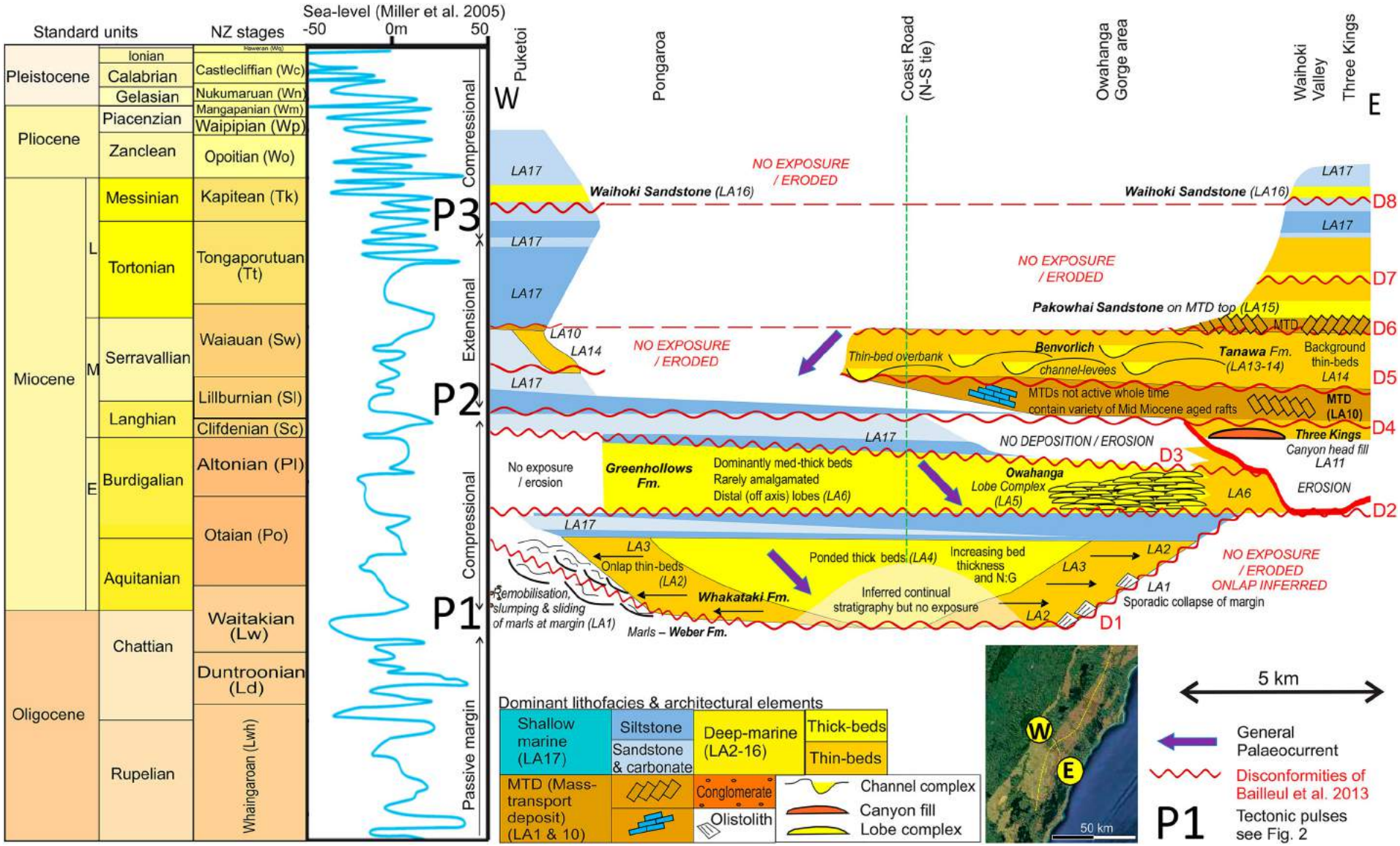

Figure 17. Chronostratigraphic chart from east to west across the basin.

sandstones (LF20) and show lateral persistence across much of the basin, but are most prevalent in the south (Figure 5), where thick, often amalgamated deposits may represent shelf sequestration. Recurrent LF18-LF20 successions represent asymmetrical transgressive-regressive sequences, including parasequence-like packages, the stratigraphic architecture being also highlighted by the shell concentrations, some of them corresponding to onlap, backlap, downlap and toplap shell beds (sensu Hendy et al. 2006). That said, intervals of shallow marine strata, particularly those with angular unconformities are identified as major periods of bypass and outboard sediment delivery (see lithofacies distribution section below).

Stratigraphic development

The mapped lithofacies associations (Figure 5), combined with biostratigraphic data, can be used to describe the temporal and spatial distribution of depositional environments, and to construct a chronostratigraphic framework for the basin fill (Figures 16 and 17).

Unconformably overlying Oligocene marls (D1; Figures 4 and 16), the fill of the basin consists of dominantly siliciclastic sedimentary rocks (Figures 2, 4, 16, and 17), which were divided into a series of biostratigraphically constrained units by Bailleul et al. (2013). The basal fill of the basin consists of mass-wasting deposits containing clasts to olistoliths of older rocks (LA1), emplaced during basin formation (Bailleul et al. 2013). The presence of LA1 on both basin margins implies structural activity on both basin margins during its inception. These are interbedded with and succeded by a Lower Miocene turbidite dominated sucession (Bailleul et al. 2007), deposition of which was widespread across the region (the Whakataki Formation [Johnston 1980]) and measure up to several hundred metres thickness (Neef 1992a), comprising LA2, 3, 4 and 9. The presence of ponded turbidites near both basin margins also implies structural activity to confine the flows on both basin margins during its initial development. Bailleul et al. (2013) recognised a general shallowing of the stratigraphy into LA17 through the uppermost Lower Miocene strata, corresponding to the Takiritini (Johnston 1980) and Coast Road (Neef 1992b) formations, culminating in an Early Miocene unconformity (D2 in Figures 4, 16, and 17).

Above this, Early Miocene turbidite sedimentation, represented by LA5, 6, 7 and 8, resumed (the Greenhollows Formation [Neef 1992b]), which shows a general shallowing-up sequence into slope and shelf sediments (LA17). This sequence culminated in a latest Early Miocene unconformity (D3 of Bailleul et al. 2013), associated with major remobilisation of shelfal sediment and cut of a canyon (LA11), which acted as as a spill conduit connecting to the downstream basin (Figure 17).

Above this lies a major angular unconformity (D4; Figures 4, 16, and 17), which corresponds with the development of a Middle Miocene shelf (LA17; The Settlement and basal part of the Ngatara formations [Neef 1992b, 1997]) above the Takiritini, Coast Road, and Greenhollows formations. These shelf strata are primarily preserved along the north-western edge of the basin.

Following an expansion of the basin limits and drowning of the Pongaroa Block (Bailleul et al. 2013), D5 is marked by a very rapid subsidence and drowning of previous shallow-water deposits with the development of a Middle Miocene deep-marine system (the Tanawa Formation [Neef 1992a]). Sedimentation became concentrated in channels and their overbanks (LA8, 12, 13, and 14). Palaeocurrent trends in the channels generally converge on the documented spill point (Figure 6). The stratigraphy was punctuated by another angular unconformity (D6), which is overlain by shelf deposits (LA17) of the Upper Miocene Ngarata Formation (upper sandstone Member; Neef 1997) and is corellated with a second major MTD (LA10; Figures 4 and 10). This succession is terminated by a disconformity (D7; Figures 4, 16, and 17; Bailleul et al. 2013).

Subsequent deposition of the deep-water Pakowhai Sandstone over the MTD (LA15; Neef 1992a) was followed by a discontinuity (D8; Bailleul et al. 2013) and return to shallow water sediments in parts of the basin. The final deep-marine deposits, a relativley unconfined submarine fan (LA16), represented by the uppermost Miocene Waihoki Formation (Neef 1992a), are truncated by shallow water to terrigenous strata as the basin filled into the Pliocene (Bailleul et al. 2013; Figure 16).

That a significant thickness of Lower Miocene shallow marine strata exists in the south of the basin implies that an axial gradient existed, with the basin being generally shallower in the south. Sediments were routed into the basin from both the north and the south in the Early to Middle Miocene, converging on the Three Kings spill point (McArthur and McCaffrey 2019). However, a levelling out and eventual reversing of the axial gradient is seen in the Upper Miocene strata, when palaeocurrents became dominantly southwards (Figure 16).

Discussion

Comparison with the fill of the Akitio Trough

The stratigraphic development of the Akitio Sub-basin (Figure 1) can be compared with the actively filling, offshore trench-slope basins, where seismic data allows examination of the architecture of these less

deformed basins. McArthur et al. (2020) described the fill of the Akitio Trough, a presently filling trench-slope basin, which demonstrates three main input channels and an evolution of the stratigraphic architecture (Figure 18). Although a subtly different setting, with no shallow marine incursions, a similar stratigraphic evolution to the outcropping basin, from confined to semi- to unconfined fill, may be distinguished (Figure 18).

The question arises as to whether the interior, outcropping basins are good analogues for the exterior, offshore basins. The interior basins formed over pre-existing thickened crust (Field et al. 1997), whereas exterior basins are forming over thinner, oceanic crust, accreted from the Pacific Plate (Barnes et al. 2018); this may lead to a different structural style, e.g. thick-skinned deformation in the interior and thin-skinned in the exterior. Evidence for this is seen in the great variation in the morphology of active basins both laterally and longitudinally across the margin (Figure 1). Furthermore, the relative proximity to the palaeoshore, water depth, slope gradient, and contour current activity have varied significantly, further complicating the style of sedimentation, potential distribution pathways, and resulting fill of trench-slope basins.

Notwithstanding some obvious differences between different slope-basins in various settings, they are always elongated, constrained by the tectonic activity that plays a major role on the development of their borders and on their sediment pathways, and which influence their confinement. The size of basins and ridges may change notably with the tectonic style (thick-

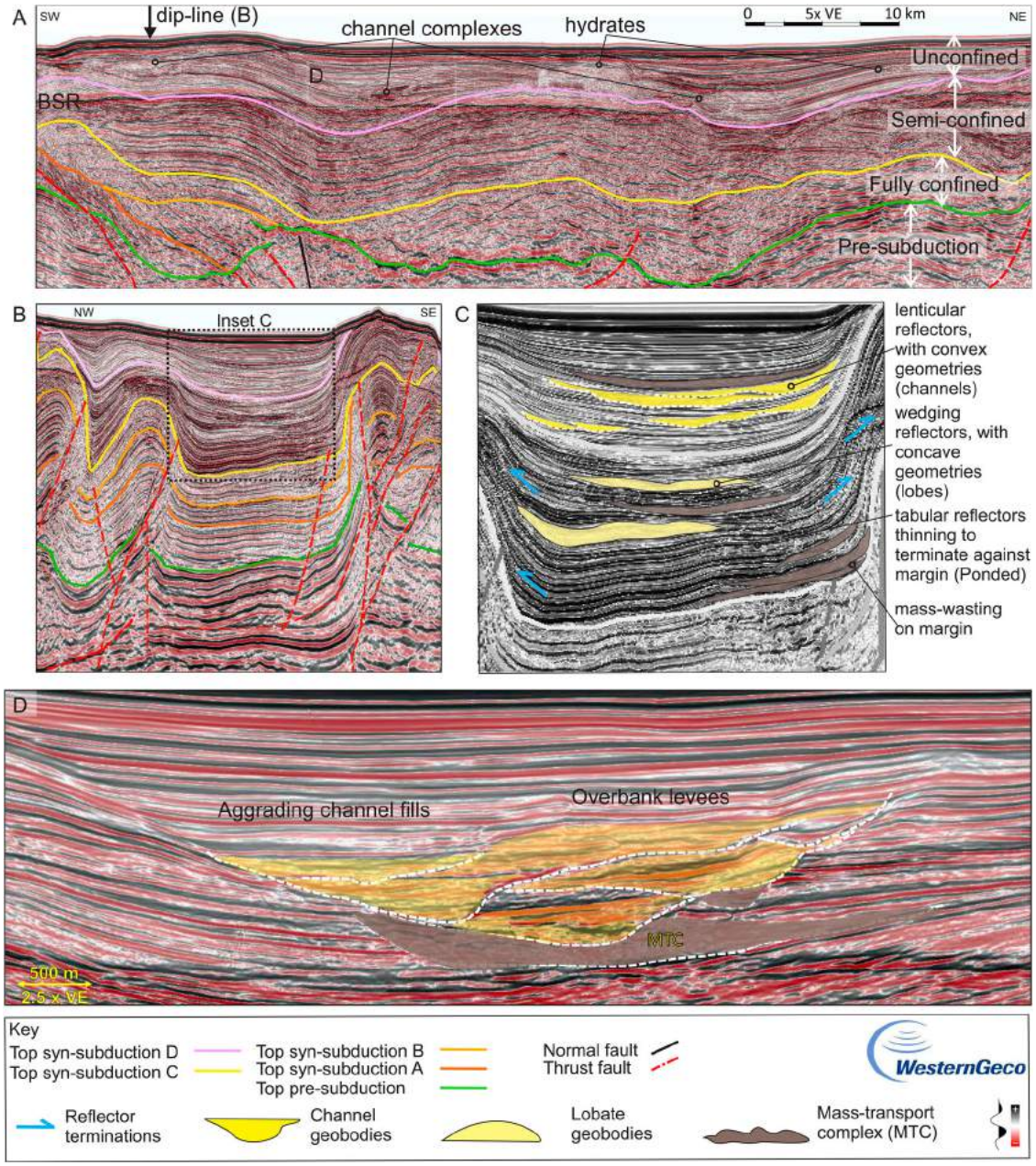

Figure 18. A, Strike-line along the Akitio Trough (Figure 1) and **B,** dip-line modified from McArthur et al. (2020), both to same scale. **C,** Interpretation of trough fill. **D,** Detail of channel-levee complex near the top of the basin fill. Syn-subduction units refer to those defined by McArthur et al. (2020). BSR – Bottom simulating reflector.

skinned vs thin-skinned) and their age varies with the proximity of the subduction trench, but their progressive sedimentary and tectonic development, linked to the subduction process is highly comparable.

That the first-order style of basin fill is similar, evolving from ponded to partly confined, to unconfined, suggest that trench-slope basins – at least on the Hikurangi Margin – share a generic pattern of fill; the fill of the Porangahau Trough also shows this type of stratigraphic evolution (McArthur et al. 2021). However, variation in trench-slope basin fill is seen, both on this margin (e.g. Burgreen and Graham 2014) and on other margins (e.g. Cascadia [Nelson et al. 2000] or the Makran [Bourget et al. 2011]). Such variation may be explained by factors including subtle differences in sediment supply, timing and style of deformation, different subduction parameters, and variable sedimentary processes, such as the recently active contour currents on this margin (Bailey et al. 2021). Nonetheless, the trench-slope basins appear to act as effective filters, trapping sediment before it reaches the trench in many subduction margins of the world (e.g. the Japan Trench [von Huene et al. 1982]). The comparison described here allows refinement on the general evolution of trench-slope basin fill.

Styles of trench-slope basin fill

New insights for the fill of trench-slope basins are presented by this study and supplement existing models (e.g. Underwood and Bachman 1982; Underwood and Moore 1995; Vinnels et al. 2010; Bailleul et al. 2013). The detailed description of the stratigraphic evolution from the outcropping Akitio Sub-basin (Figures 16 and 17) is corroborated by seismic scale studies of the offshore Akitio Trough (Figure 18). These reveal distinctive changes in style of sedimentation (Figure 19). Initially, basins form a narrow

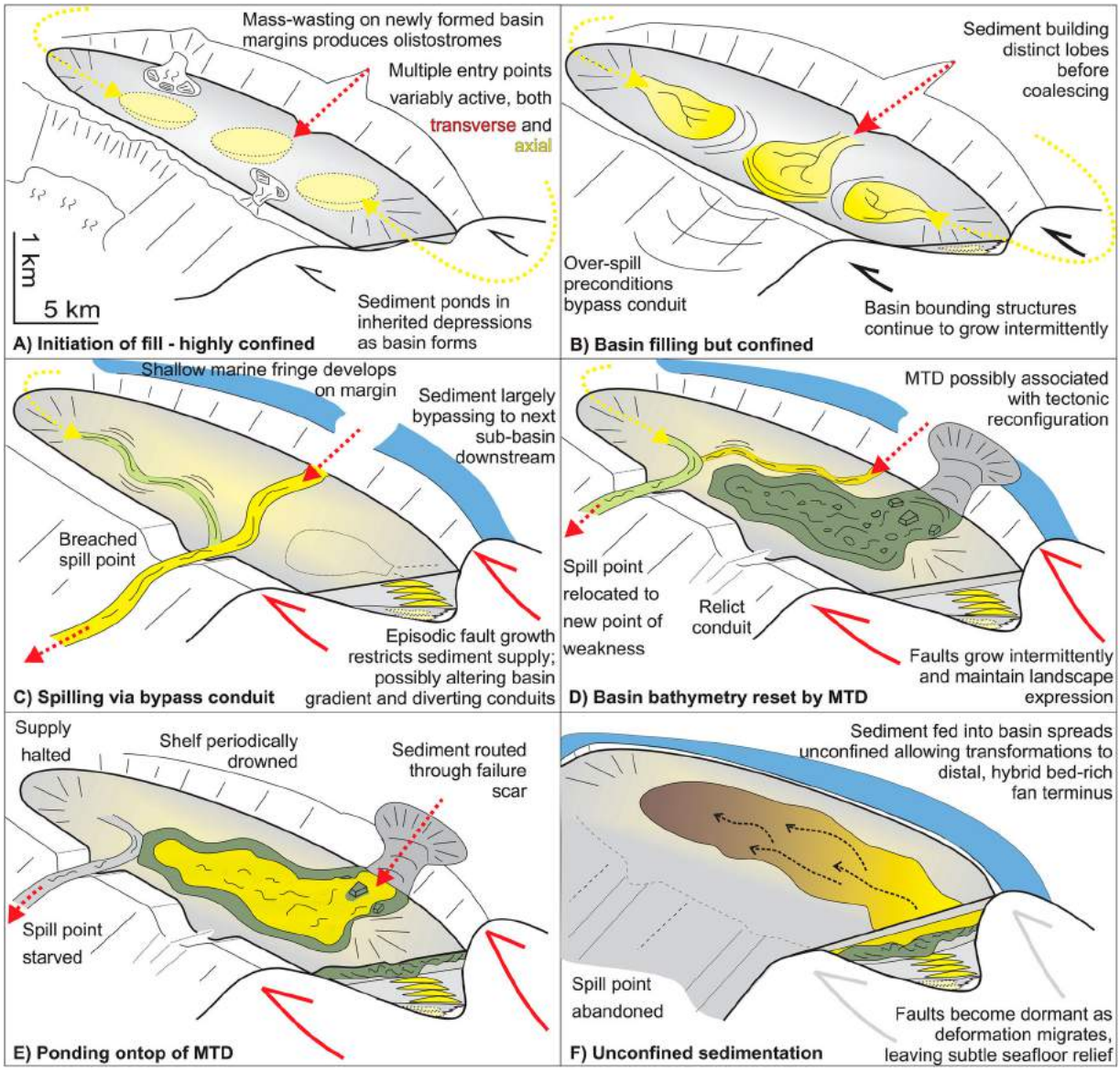

Figure 19. Schematic evolution of the fill of a trench-slope basin on the Hikurangi Margin. Although faults will not be continually active, their influence on bathymetry is likely long-lived as shown in this schematic illustration.

trough where sediments were ponded and mass-wasting occurs on newly formed basin margins (Figure 19A). Although one may expect activity first on the up-dip basin bounding structure later followed by activity on the down-dip structure, here, as with other basins on this margin (Claussmann et al. 2021), activity on both basin bounding structures is documented at basin inception. This complex structural history may result from the reactivation of older structures that define the basins (Pettinga 1982). As basins fill deposits become less confined, with lobe (Figure 19B) and subsequently channel-levee systems demonstrating a semi-confined, tortuous phase of basin evolution, with significant bypass of material outboard, via spill conduits (Figure 19C). Tectonic reconfigurations may be accompanied by emplacement of major, basin wide MTDs (Figure 19D), which may result in sediment then being trapped upon the MTD topography (Figure 19E). The final basin fill demonstrates expansion and merger of depocentres, with less confined sedimentation before the terminal fill stage basin evolution (Figure 19F).

Although documented on other margins (e.g. the Apennines [Marini et al. 2016] or the Gulf of Mexico [Sylvester et al. 2015]), the transition from fully ponded, to semi-confined, then unconfined sedimentation documented on the Hikurangi Margin offers new insights into the stratigraphic architecture of trench-slope basin fill on ocean facing margins. Here multiple sediment entry points to each basin are observed (Figures 5 and 18), leading to the development of complex stratigraphic architectures during the early stage of basin fill, which is in contrast to many simpler scenarios, where only one entry point has been described (e.g. Amy et al. 2007). The detailed outcrop descriptions from the Akitio Sub-basin may then provide a useful analogue to other subsurface systems of similar complexity, particularly when used in conjunction with comparable subsurface data (Figure 18).

As with the entry points, multiple spill points have been observed in the basin (Figure 19), implying these are not fixed as has been inferred on other margins (e.g. Gulf of Mexico [Prather et al. 2012] and offshore Nigeria [Pirmez et al. 2000]). The variety of sediment pathways leads to a diverse, heterogeneous fill of basins, i.e. which are not uniform in their fill, either temporally or spatially, with implications for resource distribution in such basins. As always, local variations, such as fault style, duration of activity, sediment flux, climate etc., will undoubtedly result in some variation in basin style and fill.

The recognition of canyons bypassing areas of the slope is a further complication, with the potential for these systems to bypass the interior portion and feed sediment directly to otherwise starved areas of the slope (Figure 19). Hence, these conduits are particularly important for concentrating and distributing the best reservoir quality sediment along the margin (McArthur et al. 2021). On the Hikurangi Margin potential reservoir sediment is largely concentrated within the trench-slope basins. Conversely, structurally defined bounding anticlines are mostly composed of deformed pre-subduction fine-grained rocks draped by syn-subduction fines, both on- (e.g. Field et al. 1997) and offshore (Ghisetti et al. 2016). Hence, there is a need to re-think classical models of drilling on structural highs in this context, both for conventional hydrocarbons and for unconventional resources, such as hydrates (Figure 18).

Controls on trench-slope basin sedimentation

Variations in sediment pathways and distribution described here can be interpreted to reflect the operation of external controls on the development of the margin, e.g. climate, tectonics, and sea-level change, which provide a first order control on basin formation, fill, and exhumation. In particular, the rapid variation between shallow and deep-marine sedimentation seen in the Akitio Sub-basin may be the result of several controls, possibly working in combination (Figure 16). The first shallow marine incursion was interpeted by Bailleul et al. (2013) to represent an episode of compression; given a rapid shift from bathyal (>1000 m water depth) to shallow water (<200 m), this event must likely represents the culmination of the first phase of convergence (Figure 2; Chanier and Ferriere 1991).

However, repeated fluctuations between deep and shallow water cannot be so simply explained. Potential mechanisms include porpoising of the basin, proposed for the Baja margin by Busby (2004); variation in orientation and speed of subduction (e.g. Nicol et al. 2007); episodes of underplating, inferred to be responsible for similar sequences around the Mediterranean (Puigdefabregas et al. 1992); out-of-sequence deformation (Chanier and Ferriere 1991); or local anomalies, e.g. basement fabric (Barnes et al. 2020). Another possible mechanism could be seamount subduction (e.g. Dominguez et al. 1998). However, unless associated with subduction of very large seamounts, the effect should be relatively laterally localised to the width of the seamount and not applicable to processes along the length of the margin. This remains a topic for further study. Evidence of transgressive-regressive sequences and parasequences in the shallow marine successions (e.g. LF19) indicates eustatic sea-level fluctuations were also influencing the sedimentation. The fluctuation between shelfal water depths (~200 m) and upper bathyal depths (~400 m) in the terminal basin fill may be related to sea-level and sediment supply fluctuations, rather than purely tectonic events. Ultimately, the uplift and exhumation of the Akitio Sub-basin was driven by tectonics.

At a second order, the filling-up megasequence evolution from under- to overfilled dictates the overall style of sedimentation within a basin, but itself is not simply progressive, with various stages of 'filling' and 'spilling' of the basin. At the third order, local regulators on the sedimentary system, e.g. formation of spill points, local variation in structures, or distribution of MTDs, affect the lateral and longitudinal distribution of sediment. The basin-wide unconformities and MTDs seen in the Middle and Upper Miocene strata represent major changes in the depositional system of the Akitio Sub-basin (Figure 15). The MTDs may be the cause of such changes, however, the MTDs themselves were likely triggered by an external event (Claussmann et al. 2021). The Middle Miocene MTD can be correlated with a major tectonic pulse in the basin (Figure 16). However, the major Upper Miocene MTD does not correlate with a described tectonic event, but does appear to coincide with a major sea-level fall (Figure 16), which has been linked to shelf and slope destabilisation on other margins (Moscardelli and Wood 2008).

Conclusions

An updated description of the fill the onshore Akitio Sub-basin, Wairarapa, New Zealand, an exhumed trench-slope basin, was enabled by new stratigraphic sections and geological mapping. A heterolithic range of sedimentary rocks was encountered across the basin fill, varying laterally, longitudinally, and vertically. Sedimentation in the basin is thus documented to have varied both temporally and spatially as depocentres were created, filled, and became overfilled, resulting in a fully, to semi-, to unconfined stratigraphic evolution. The development of intervals of shallow marine strata, particularly those capped by unconformities, is highlighted as indicating episodes of potential reworking and bypass of sediment outboard through spill conduits; significant bypass likely occurred in the mid Early Miocene, the early Middle Miocene, and the latest Miocene.

Integration of field data with bathymetric data and data derived from offshore seismic studies from the same margin shows that similar sedimentary systems were active elsewhere on the margin during the Neogene and are still active today. Fundamentally, three levels of control determine the fill of trench-slope basins. At the highest order, external controls, i.e. tectonics and climate, determine creation (and demise) of a basin, its sediment supply, and its deformation; a second-order control reflects its progression from under- to overfilled; a third-order lateral variation reflects the effects of local process (e.g. formation of spill points) and/or the effects of tectonics on the location of structures and internal basin-gradients. The models of trench-slope basin fill developed here may aid understanding of basins in similar settings with limited preservation or less data.

Acknowledgements

This research was funded by a JIP between Chevron, Equinor, OMV and Schlumberger at the University of Leeds. WesternGeco are thanked for permission to show seismic sections. Thanks to field assistants Vanisha Pulan and Nick Zajac, David Francis of Geological Research for an introduction to the field area, and land owners for permission to access the field sites. Finally, we thank Editor Kyle Bland and reviewers Christopher Uruski and Dominic Strogen for their helpful comments and suggestions.

Disclosure statement

No potential conflict of interest was reported by the author(s).

Data availability statement

The data that support the findings of this study are available from the corresponding author upon request.

References

Amorosi A. 1995. Glaucony and sequence stratigraphy: a conceptual framework of distribution in siliciclastic sequences. Journal of Sedimentary Research. 65:419–425.

Amy LA, Kneller BC, McCaffrey WD. 2007. Facies architecture of the Gres de Peira Cava, SE France: landward stacking patterns in ponded turbiditic basins. Journal of the Geological Society. 164:143–162.

Bailey WS, McArthur AD, McCaffrey WD. 2021. Distribution of contourite drifts on convergent margins: Examples from the Hikurangi subduction margin of New Zealand. Sedimentology. 68:294–323.

Bailleul J, Robin C, Chanier F, Guillocheau F, Field B, Ferriere J. 2007. Turbidite systems in the inner forearc domain of the Hikurangi convergent margin (New Zealand): New constraints on the development of Trench-Slope Basins. Journal of Sedimentary Research. 77:263–283. DOI:10.2110/jsr.2007.028.

Bailleul J, Chanier F, Ferrière J, Robin C, Nicol A, Mahieux G, Gorini C, Caron V. 2013. Neogene evolution of lower trench-slope basins and wedge development in the central hikurangi subduction margin, New Zealand. Tectonophysics. 591:152–174. DOI:10.1016/j.tecto.2013.01.003.

Ballance PF. 1976. Evolution of the Upper Cenozoic magmatic arc and plate boundary in northern New Zealand. Earth and Planetary Science Letters. 28:356–370.

Barnes PM, Nicol A, Harrison T. 2002. Late Cenozoic evolution and earthquake potential of an active listric thrust complex above the Hikurangi subduction zone, New Zealand. Geological Society of America Bulletin. 114:1379–1405.

Barnes PM, Lamarche G, Bialas J, Henrys S, Pecher I, Netzeband GL, Greinert J, Mountjoy JJ, Pedley K, Crutchley G. 2010. Tectonic and geological framework for gas hydrates and cold seeps on the Hikurangi subduction margin, New Zealand. Marine Geology, 272:26–48.

Barnes PM, Ghisetti FC, Ellis S, Morgan JK. 2018. The role of protothrusts in frontal accretion and accommodation of plate convergence, Hikurangi subduction margin, New Zealand. Geosphere. 14:440–468.

Barnes PM, Wallace LM, Saffer DM, Bell RE, Underwood MB, Fagereng A, Meneghini F, Savage HM, Rabinowitz HS, Morgan JK, Kitajima H. 2020. Slow slip source characterized by lithological and geometric heterogeneity. Science Advances. 6:p.eaay3314.

Beanland S, Melhuish A, Nicol A, Ravens J. 1998. Structure and deformational history of the inner forearc region, Hikurangi subduction margin, New Zealand. New Zealand Journal of Geology and Geophysics. 41:325–342. DOI:10.1080/00288306.1998.9514814.

Bland KJ, Uruski CI, Isaac MJ. 2015. Pegasus Basin, eastern New Zealand: A stratigraphic record of subsidence and subduction, ancient and modern. New Zealand Journal of Geology and Geophysics. 58:319–343.

Bourget J, Zaragosi S, Ellouz-Zimmermann N, Mouchot N, Garlan T, Schneider JL, Lanfumey V, Lallemant S. 2011. Turbidite system architecture and sedimentary processes along topographically complex slopes: the Makran convergent margin. Sedimentology. 58:376–406.

Brodie JW, Hatherton T. 1958. The morphology of Kermadec and Hikurangi trenches. Deep Sea Research (1953). 5:18–IN2.

Burgreen-Chan B, Meisling KE, Graham S. 2016. Basin and petroleum system modelling of the East Coast Basin, New Zealand: a test of overpressure scenarios in a convergent margin. Basin Research. 28:536–567. DOI:10.1111/bre.12121.

Burgreen B, Graham S. 2014. Evolution of a deep-water lobe system in the Neogene trench-slope setting of the East Coast Basin, New Zealand: lobe stratigraphy and architecture in a weakly confined basin configuration. Marine and Petroleum Geology. 54:1–22. DOI:10.1016/j.marpetgeo.2014.02.011.

Busby C. 2004. Continental growth at convergent margins facing large ocean basins: a case study from Mesozoic convergent-margin basins of Baja California, Mexico. Tectonophysics. 392:241–277.

Butler RWH. 2019. Syn-kinematic strata influence the structural evolution of emergent fold-thrust belts. Geological Society. London, Special Publications, 490:SP490.

Caron J, Bailleul J, Chanier F, Mahieux G. 2021. Episodes of seabed rise and rapid drowning as primary controls for the development of regressive and transgressive heterozoan carbonates and rhodolithic limestones in a tectonically-active setting (Early Miocene, Wairarapa region, New Zealand). New Zealand Journal of Geology and Geophysics. DOI:10.1080/00288306.2021.1960865.

Chanier F, Ferriere J. 1991. From a passive to an active margin; tectonic and sedimentary processes linked to the birth of an accretionary prism (Hikurangi Margin, New Zealand). Bulletin de la Société Géologique de France. 162:649–660.

Chanier F, Ferrière J, Angelier J. 1999. Extensional deformation across an active margin, relations with subsidence, uplift, and rotations: The Hikurangi subduction, New Zealand. Tectonics. 18:862–876. DOI:10.1029/1999TC900028.

Clark IR, Cartwright JA. 2012. Interactions between coeval sedimentation and deformation from the Niger Delta Deepwater Fold Belt. In: Prather BE, Deptuck ME, Mohrig D, Van Hoorn B, Wynn RB, editors. Application of the principles of seismic geomorphology to continental-slope and base-of-slope systems: case studies from seafloor and near-seafloor analogues. City: SEPM Special Publication, Vol. 99; p. 243–267.

Claussmann B, Bailleul J, Chanier F, Mahieux G, Caron V, McArthur AD, Chaptal C, Morgans H, Vendeville BC. 2021. Shelf-derived mass-transport deposits: origin and significance in the stratigraphic development of trench-slope basins. New Zealand Journal of Geology and Geophysics. DOI:10.1080/00288306.2021.1918729.

Clowes CD, Crampton JS, Bland KJ, Collins KS, Prebble JG, Raine JI, Strogen DP, Terezow MG, Womack T. 2021. The New Zealand fossil record file: a unique database of biological history. New Zealand Journal of Geology and Geophysics. 64:62–71.

Cohen KM, Finney SC, Gibbard PL, Fan J-X. 2013. The ICS international chronostratigraphic chart. Episodes. 36:199–204.

Crisóstomo-Figueroa A, McArthur AD, Dorrell RM, Amy L, McCaffrey WD. 2020. A new modelling approach to sediment bypass prediction applied to the East Coast Basin, New Zealand. GSA Bulletin. DOI:10.1130/B35687.1.

Crowell JC. 1957. Origin of pebbly mudstones. Geological Society of America Bulletin. 68:993–1010. ``

Delteil J, de Lepinay BM, Morgans HEG, Field BD. 2006. Olistostromes marking tectonic events, East Coast, New Zealand. New Zealand Journal of Geology and Geophysics. 49:517–531. DOI:10.1080/00288306.2006.9515185.

Dominguez S, Lallemand SE, Malavieille J, von Huene R. 1998. Upper plate deformation associated with seamount subduction. Tectonophysics. 293:207–224.

Dott RH, Bourgeois J. 1982. Hummocky stratification: significance of its variable bedding sequences. GSA Bulletin. 93:663–680.

Field BD, Uruski CI, Beu AG, Browne GH, Crampton JS, Funnell R, Killops S, Laird MG, Mazengarb C, Morgans HEG, et al. 1997. Cretaceous–Cenozoic geology and petroleum systems of the East Coast region, New Zealand: New Zealand Institute of Geological and Nuclear Sciences, Monograph 19, 301 pp.

Francis DA, Johansen A. 2011. Geology of the Kawakawa Structure: New Zealand Petroleum and Minerals, Ministry of Economic Development New Zealand Unpublished Report, PR4482, 48 pp.

Galloway WE. 1998. Siliciclastic slope and base-of-slope depositional systems: component facies, stratigraphic architecture, and classification. AAPG Bulletin. 82:569–595.

Ghisetti FC, Barnes PM, Ellis S, Plaza-Faverola AA, Barker DH. 2016. The last 2 Myr of accretionary wedge construction in the central Hikurangi margin (North Island, New Zealand): insights from structural modeling. Geochemistry, Geophysics, Geosystems. 17:2661–2686.

Haughton PDW, Barker SP, McCaffrey WD. 2003. Linked debrites in sand-rich turbidite systems – origin and significance. Sedimentology. 50:459–482. DOI:10.1046/j.1365-3091.2003.00560.x.

Hendy AJW, Kamp PJJ, Vonk AJ. 2006. Cool-water shell bed taphofacies from Miocene-Pliocene shelf sequences in New Zealand: utility of taphofacies in sequence stratigraphic analysis. In: Pedley HM, Carannante G, editors. Cool-water carbonates: depositional systems and palaeoenvironmental controls. London: Geological Society of London Special Publications; Vol. 255, p. 283–305.

Heron, DW (custodian). 2014. Geological map of New Zealand 1:250,000. Lower Hutt, NZ: GNS Science. GNS Science geological map. 1 CD.

Hubbard SM, Romans BW, Graham SA. 2008. Deep-water foreland basin deposits of the Cerro Toro Formation, Magallanes Basin, Chile; architectural elements of sinuous basin axial channel belt. Sedimentology. 55:1333–1359.

Jiao R, Seward D, Little TA, Kohn BP. 2014. Thermal history and exhumation of basement rocks from Mesozoic to Cenozoic subduction cycles, central North Island, New Zealand. Tectonics. 33:1920–1935.

Jobe ZR, Lowe DR, Morris WR. 2012. Climbing-ripple successions in turbidite systems: depositional environments, sedimentation rates and accumulation times. Sedimentology. 59:867–898.

Johansen AC. 1999. Geology of the Upper Tinui Valley area, Wairarapa. Unpublished BSc (Hons) thesis, Victoria University of Wellington. 166 pp.

Johnston MR. 1980. Geology of the Tinui-Awatoitoi district: New Zealand Department of Scientific and Industrial Research, v. 94, 61 pp.

Kane IA, Hodgson DM. 2011. Sedimentological criteria to differentiate submarine channel levee subenvironments: exhumed examples from the Rosario Fm. (Upper Cretaceous) of Baja California, Mexico, and the Fort Brown Fm. (Permian), Karoo Basin, S. Africa. Marine and Petroleum Geology. 28:807–823. DOI:10.1016/j.marpetgeo.2010.05.009.

Kane IA, Pontén A, Vangdal B, Eggenhuisen J, Hodgson DM, Spychala YT. 2016. The stratigraphic record and processes of turbidity current transformation across deep-marine lobes. Sedimentology. DOI:10.1111/sed.12346.

Kingma JT. 1958. The tongaporutuan sedimentation in central Hawke's Bay. New Zealand Journal of Geology and Geophysics. 1:1–30.

Kneller B, Dykstra M, Fairweather L, Milana JP. 2016. Mass-transport and slope accommodation: implications for turbidite sandstone reservoirs. AAPG Bulletin. 100:213–235.

Kneller B, McCaffrey W. 1999. Depositional effects of flow nonuniformity and stratification within turbidity currents approaching a bounding slope; deflection, reflection, and facies variation. Journal of Sedimentary Research. 69:980–991.

Lee JM, Begg JG. 2002. Geology of the Wairarapa area: Institute of Geological & Nuclear Sciences 1:250,000 geological map 11. 1 sheet + 66 pages. Institute of Geological and Nuclear Sciences Ltd, Lower Hutt, New Zealand.

Lewis KB, Pettinga JR. 1993. The emerging, imbricate frontal wedge of the Hikurangi margin. In: Balance PF, editor. Sedimentary basins of the world. New York: Elsevier. Vol. 2, p. 225–250.

Lillie AR. 1953. The geology of the Dannevirke Subdivision: Wellington: Department of Scientific and Industrial Research. New Zealand Geological Survey bulletin 46, 156 p.

Litchfield N, Ellis S, Berryman K, Nicol A. 2007. Insights into subduction-related uplift along the Hikurangi Margin, New Zealand, using numerical modeling. Journal of Geophysical Research: Earth Surface. 112:1–17.

Lowe DR. 1982. Sediment gravity flows; II. depositional models with special reference to the deposits of high-density turbidity currents. Journal of Sedimentary Petrology. 52:279–297.

Malié P, Bailleul J, Chanier F, Toullec R, Mahieux G, Caron V, Field B, Mählmann RF, Potel S. 2017. Spatial distribution and tectonic framework of fossil tubular concretions as onshore analogues of cold seep plumbing systems, North Island of New Zealand. Bulletin de la Société Géologique de France. 188:25.

Marini M, Felletti F, Milli S, Patacci M. 2016. The thick-bedded tail of turbidite thickness distribution as a proxy for flow confinement: Examples from tertiary basins of central and northern Apennines (Italy). Sedimentary Geology. 341:96–118.

McArthur AD, McCaffrey WD. 2019. Sedimentary architecture of detached deep-marine canyons: Examples from the East Coast Basin of New Zealand. Sedimentology. 66:1067–1101.

McArthur AD, Tek DE. 2021. Controls on the origin and evolution of deep-ocean trench-axial channels. Geology. DOI:10.1130/G48612.1.

McArthur AD, Claussmann B, Bailleul J, Clare A, McCaffrey WD. 2020. Variation in syn-subduction sedimentation patterns from inner to outer portions of deep-water fold and thrust belts: examples from the Hikurangi subduction margin of New Zealand. In: Hammerstein JA, Di Cuia R, Cottam MA, Zamora G, Butler RWH, editors. Geological society. London: Special Publications; 490(1), p. 285–310.

McArthur AD, Bailleul J, Mahieux G, Claussmann B, Wunderlich A, McCaffrey WD. 2021. Deformation-sedimentation feedback and the development of anomalously thick aggradational turbidite lobes: outcrop and subsurface examples from the Hikurangi Margin, New Zealand. Journal of Sedimentary Research. DOI:10.2110/jsr.2020.013.

Miller KG, Kominz MA, Browning JV, Wright JD, Mountain GS, Katz ME, Sugarman PJ, Cramer BS, Christie-Blick N, Pekar SF. 2005. The Phanerozoic record of global sea-level change. Science. 310:1293–1298.

Morley CK, King R, Hillis R, Tingay M, Backe G. 2011. Deepwater fold and thrust belt classification, tectonics, structure and hydrocarbon prospectivity: a review. Earth-Science Reviews. 104:41–91.

Moscardelli L, Wood L. 2008. New classification system for mass transport complexes in offshore Trinidad. Basin Research. 20:73–98.

Mountjoy JJ, Micallef A. 2012. Polyphase emplacement of a 30 km 3 blocky debris avalanche and its role in slope-gully development. In: Yamada Y, Kawamura K, Ikehara K, Ogawa Y, Urgeles R, Mosher D, Chaytor J, Strasser M, editors. Submarine mass movements and their consequences. New York: Springer; p. 213–222.

Neef G. 1967. The Geology of Eketahuna: Victoria University of Wellington, 493 p.

Neef G. 1981. Structure of NZMS1 N153 Eketahuna sheet district and tectonics of Northern Wairarapa, North Island, New Zealand. New Zealand Journal of Geology and Geophysics. 24:603–613.

Neef G. 1991. A clastic dike-sill assemblage in late Miocene (c. 6 Ma) strata, Annedale, Northern Wairarapa, New Zealand. New Zealand Journal of Geology and Geophysics. 34:87–91.

Neef G. 1992a. Turbidite deposition in five miocene, bathyal formations along an active plate margin, North Island, New Zealand: with notes on styles of deposition at the margins of east coast Bathyal basins. Sedimentary Geology. 78:111–136.

Neef G. 1992b. Geology of the Akitio area (1: 50 000 metric sheet U25BD, east), northeastern Wairarapa, New Zealand. New Zealand Journal of Geology and Geophysics. 35:533–548.

Neef G. 1995. Cretaceous and Cenozoic geology east of the Tinui Fault Complex in northeastern Wairarapa. New

Zealand: New Zealand Journal of Geology and Geophysics. 38:375–394.
Neef G. 1997. Stratigraphy, structural evolution, and tectonics of the northern part of the Tawhero Basin and adjacent areas, northern Wairarapa, North Island, New Zealand. New Zealand Journal of Geology and Geophysics. 40:335–358.
Neef G. 1999a. Late Miocene marine fossil-rich, rock-fall, avalanche, mud-flow and debris-flow deposits adjoining and near the western margin of the Tawhero Basin, outer forearc North Island, New Zealand: transactions of the Royal Society of Edinburgh. Earth Sciences. 90:189–201.
Neef G. 1999b. Neogene development of the onland part of the forearc in northern Wairarapa, North Island, New Zealand: a synthesis. New Zealand Journal of Geology and Geophysics. 42:113–135.
Neef G, Bottrill RS. 1992. The Cenozoic geology of the Gisborne area (1: 50 000 metric sheet Y18AB), North Island, New Zealand. New Zealand Journal of Geology and Geophysics. 35:515–531.
Nelson CH, Goldfinger C, Johnson JE, Dunhill G. 2000. Variation of modern turbidite systems along the subduction zone margin of Cascadia basin and implications for turbidite reservoir beds. In: Weimer P., editor. Deep-Water Reservoirs of the World: 20th Annual Research Conference, Gulf Coast Section Society of Economic Paleontologists and Mineralogists. Tulsa (OK): SEPM. p. 714–738.
Nicol A, Beavan J. 2003. Shortening of an overriding plate and its implications for slip on a subduction thrust, central Hikurangi Margin, New Zealand. Tectonics. 22.
Nicol A, Mazengarb C, Chanier F, Rait G, Uruski C, Wallace L. 2007. Tectonic evolution of the active Hikurangi subduction margin, New Zealand, since the Oligocene. Tectonics. 26:1–24.
Ongley M. 1935. Eketahuna subdivision: New Zealand Geological Survey 29th annual report (ns) 1934–I935, p. 1–6.
Patacci M, Haughton PDW, Mccaffrey WD. 2015. Flow behavior of ponded turbidity currents. Journal of Sedimentary Research. 85:885–902.
Pettinga JR. 1982. Upper Cenozoic structural history, coastal southern Hawkes Bay, New Zealand. New Zealand Journal of Geology and Geophysics. 25:149–191.
Pirmez C, Beaubouef RT, Friedmann SJ, Mohrig DC. 2000. Equilibrium profile and baselevel in submarine channels: Examples from Late Pleistocene Systems and implications for the Architecture of Deepwater Reservoirs. In: GCSSEPM Foundation 20th Annual Research Conference, Deep-Water Reservoirs of the World. Tulsa (OK): SEPM. p. 782–805.
Posamentier HW. 2003. Depositional elements associated with a basin floor channel-levee system: case study from the Gulf of Mexico. Marine and Petroleum Geology. 20:677–690.
Prather BE, Pirmez C, Winker CD. 2012. Stratigraphy of Linked Intraslope Basins: Brazos-Trinity System Western Gulf of Mexico. In: Prather B. E., Deptuck M. E., Mohrig D., Van Hoorn B., Wynn R. B., editor. Application of the principles of seismic geomorphology to continental-slope and base-of-slope systems: Case studies from seafloor and near-seafloor analogues. Tulsa (OK): SEPM Special Publication; 99, p. 83–109.
Prelat A, Hodgson DM, Flint SS. 2009. Evolution, architecture and hierarchy of distributary deep-water deposits: a high-resolution outcrop investigation from the Permian Karoo Basin, South Africa. Sedimentology. 56:2132–2154.
Puigdefabregas C, Muñoz JA, Verges J. 1992. Thrusting and foreland basin evolution in the Southern Pyrenees. In: K.R. McClay, editor. Thrust tectonics. London: Chapman & Hall; p. 247–254.
Rait G, Chanier F, Waters DW. 1991. Landward- and seaward-directed thrusting accompanying the onset of subduction beneath New Zealand. Geology. 19:230–233.
Raine JI, Beu AG, Boyes AF, Campbell H, Cooper RA, Crampton JS, Crundwell MP, Hollis CJ, Morgans HEG. 2015. Revised calibration of the New Zealand Geological Timescale: NTGT2015/1: GNS Science Lower Hutt.
Reid CM. 1998. Stratigraphy, paleontology, and tectonics of lower Miocene rocks in the Waipatiki/Mangatuna area, southern Hawke's Bay, New Zealand. New Zealand Journal of Geology and Geophysics. 41:115–131.
Reyners M. 2013. The central role of the Hikurangi Plateau in the Cenozoic tectonics of New Zealand and the Southwest Pacific. Earth and Planetary Science Letters. 361:460–468.
Stevenson CJ, Jackson CA-L, Hodgson DM, Hubbard SM, Eggenhuisen JT. 2015. Deep-water sediment bypass. Journal of Sedimentary Research. 85:1058–1081.
Strogen DP, Bland KJ, Nicol A, King PR. 2014. Paleogeography of the Taranaki Basin region during the latest Eocene–Early Miocene and implications for the 'total drowning' of Zealandia. New Zealand Journal of Geology and Geophysics. 57:110–127.
Sylvester Z, Cantelli A, Pirmez C. 2015. Stratigraphic evolution of intraslope minibasins: insights from surface-based model. AAPG Bulletin. 99:1099–1129.
Tap Oil Limited. 2004. Tawatawa-1 Well Completion Report. New Zealand Ministry of Economic Development Petroleum Series Report 3067. New Zealand, Wellington, p. 873.
Tinterri R. 2011. Combined flow sedimentary structures and the genetic link between sigmoidal-and hummockycross stratification. GeoActa. 10:43–85.
Underwood MB, Bachman SB. 1982. Sedimentary facies associations within subduction complexes. Geological Society, London, Special Publications. 10:537–550.
Underwood MB, Moore GF. 1995. Trenches and trench-slope basins: tectonics of sedimentary basins. In: Busby C, Ingersoll RV, editors. Tectonics of sedimentary basins. Cambridge (MA): Blackwell Science. 179–219.
Uruski CI. 1997. Post-mortem on Titihaoa-1, Wairarapa. Institute of Geological and Nuclear Sciences Science Report 97/31.
Van Der Lingen GJ, Pettinga JG. 1980. The Makara basin: a Miocene slope-basin along the New Zealand sector of the Australian-Pacific obliquely convergent plate boundary. In: Ballance P.F., Reading H.G, editor. Sedimentation in Oblique-slip Mobile Zones. Intternational Association of Sedimentologists. Special Publication, 4, Oxford: Blackwell Scientific Publications; p. 191–215.
Vinnels JS, Butler RWH, McCaffrey WD, Paton DA. 2010. Depositional processes across the Sinú accretionary prism, offshore Colombia. Marine and Petroleum Geology. 27:794–809.
von Huene R, Langseth M, Nasu N, Okada H. 1982. A summary of Cenozoic tectonic history along the IPOD Japan trench transect. Geological Society of America Bulletin. 93:829–846.
Wells P. 1989. Burial history of Late Neogene sedimentary basins on part of the New Zealand convergent plate margin. Basin Research. 2:145–160.